Applied Thermal Engineering 231 (2023) 120698

Contents lists available at ScienceDirect

Applied Thermal Engineering

journal homepage: www.elsevier.com/locate/apthermeng

A transient simulation for a novel solar-geothermal cogeneration system with a selection of heat transfer fluids using thermodynamics analysis and ANN intelligent (AI) modeling

Ehsanolah Assareh [a,1,*], Siamak Hoseinzadeh [b,*], Neha Agarwal [a,1], Mostafa Delpisheh [c], Ali Dezhdar [d], Masoud Feyzi [e], Qiliang Wang [f], Davide Astiaso Garcia [b], Ehsan Gholamian [g], Mehdi Hosseinzadeh [h,*], Maryam Ghodrat [i], Moonyong Lee [a,*]

[a] School of Chemical Engineering, Yeungnam University, Gyeongsan 38541, South Korea
[b] Department of Planning, Design, and Technology of Architecture, Sapienza University of Rome, Rome 00196, Italy
[c] School of Mechanical Engineering, Iran University of Science and Technology (IUST), Tehran, Iran
[d] Young Researchers and Elite Club, Dezful Branch, Islamic Azad University, Dezful, Iran
[e] Department of Mechanical Engineering, Arvandan Non-profit Higher Education Institute, Khorramshahr, Iran
[f] Renewable Energy Research Group (RERG), Department of Building Environment and Energy Engineering, The Hong Kong Polytechnic University, Hong Kong, China
[g] Faculty of Mechanical Engineering, University of Tabriz, Tabriz, Iran
[h] Institute of Research and Development, Duy Tan University, Da Nang, Viet Nam
[i] School of Engineering and Information Technology, University of New South Wales Canberra, Canberra 2610, ACT, Australia

ARTICLE INFO

Keywords:
Solar energy
Geothermal energy
Parabolic trough solar collector
Heat transfer fluid
Exergoeconomic

ABSTRACT

Today, due to the reduction of fossil resources and on the other hand the high environmental pollution of these resources, it is necessary to pay attention to alternative resources, including clean and available renewable resources. In this study, solar and geothermal energy sources are combined, generating electricity, cooling, freshwater, and hydrogen, along with selecting a suitable heat transfer fluid for parabolic trough solar collectors. This system consists of parabolic trough solar collectors, a steam Rankine cycle, a steam Rankine cycle with an organic Rankine cycle, a proton exchange membrane electrolyzer, and a reverse osmosis desalination unit. To analyze the performance of solar collectors, Therminol 59, Marlotherm SH, Syltherm 800, and Therminol VP1 heat transfer fluids are selected. Solar radiation intensity, solar collector mass flow rate, turbine and pump efficiency, evaporator pinch-point temperature, and organic Rankine cycle turbine inlet temperature were investigated as design parameters affecting system performance. Maximizing energy efficiency and reducing cost rate were selected as two objective functions and determined using a multi-objective sorting genetic algorithm (NSGA-II). The results showed that Therminol 59 has the highest energy efficiency and net power output compared to other heat transfer fluids. Also, the proposed system produces 1140 kW of electricity in the optimal state, and in the best state, it has an energy efficiency of 32.39% and a cost of 36.32 $/GJ.

1. Introduction

The need for energy and its use in industrial and domestic applications is one of the criteria for determining the level of progress and quality of life in a country. The expansion of the need for energy sources has always been one of the important basic issues in human life, and trying to reach an inexhaustible source of energy has been one of the long-standing dreams of man. Today, societies and countries of the world are more dependent on energy than in the past decades and years. The reason is to look for ways to increase system performance and simultaneously reduce system costs and reduce environmental pollution caused by system activity and burning fossil resources as the main cause of this CO_2 emission. Currently, the energy demand is increasing in all countries of the world and this demand is also increasing day by day.

* Corresponding authors.
E-mail addresses: ehsanolah.assareh@yu.ac.kr (E. Assareh), siamak.hosseinzadeh@uniroma1.it (S. Hoseinzadeh), mehdihosseinzadeh@duytan.edu.vn (M. Hosseinzadeh), mynlee@yu.ac.kr (M. Lee).
[1] These authors contributed equally to this article as the first authors.

https://doi.org/10.1016/j.applthermaleng.2023.120698
Received 22 October 2022; Received in revised form 5 April 2023; Accepted 3 May 2023
Available online 2 June 2023

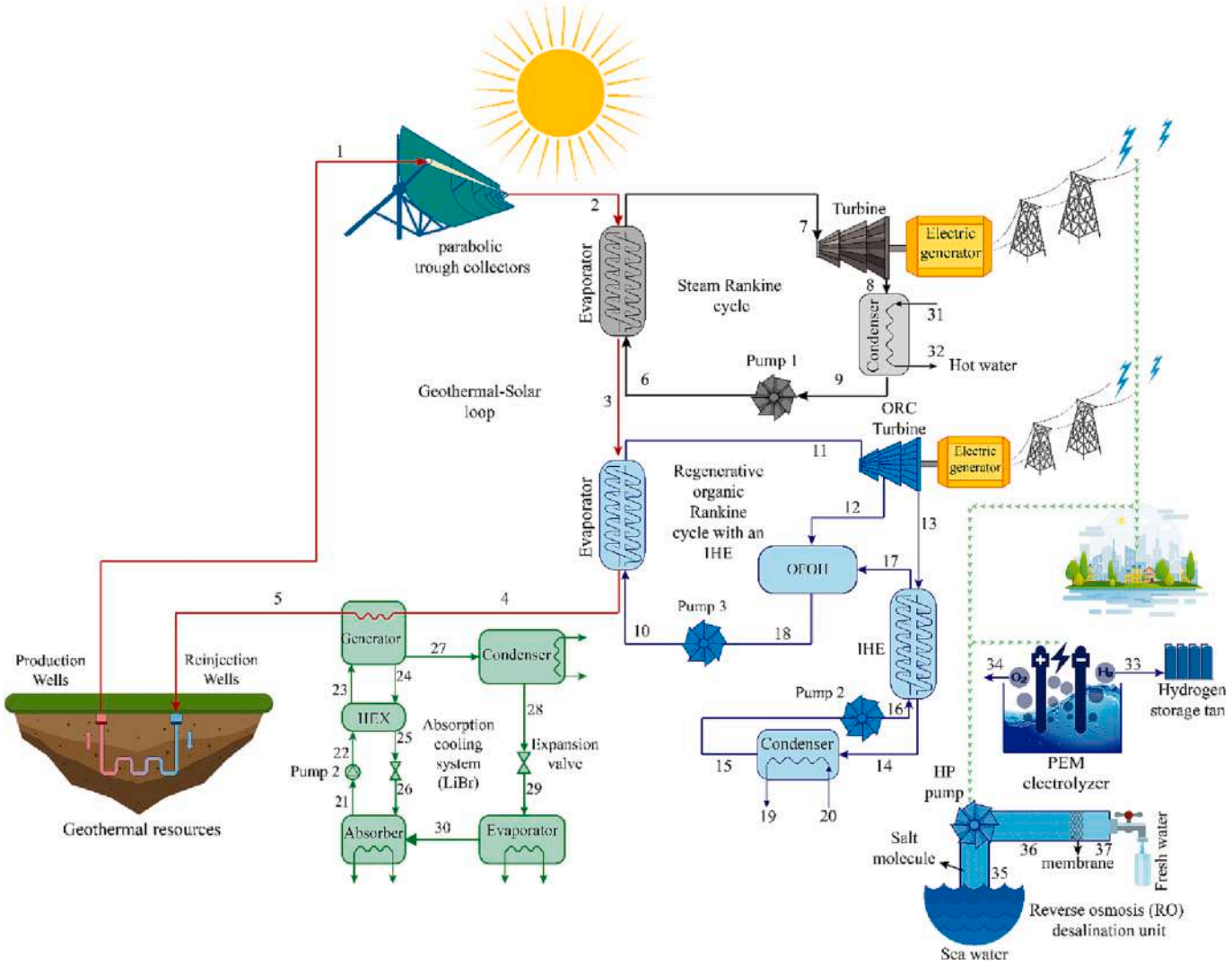

Fig. 1. Schematic process flow diagram of the proposed poly-generation system.

Table 1
Input data used in the simulation.

Parameter	Value
T_0	25 °C
P_0	101.3 [kPa]
$\dot{m}_1$	15 [kg/h]
T_{sun}	5505 [°C]
$T_{geothermal}$	190 [°C]
$\eta_{turbine}$	0.80 %
η_{pump}	0.90%
pp_{Eva}	5 [°C]
pp_{Cond}	5 [°C]
P_7	1500 [kPa]
P_9	100 [kPa]
G_b	850 [W/m^2]

Table 2
Energy balance of system components.

Components	Relation
SRC turbine	$\dot{W}_{turbine,\ steam} = \dot{m}_7 \times (h_7 - h_8)$
Pump No. 1	$\dot{W}_{pump1} = \dot{m}_6 \times (h_6 - h_9)$
Pump No. 2	$\dot{W}_{pump2} = \dot{m}_{15} \times (h_{16} - h_{15})$
Pump No. 3	$\dot{W}_{pump3} = \dot{m}_{18} \times (h_{10} - h_{18})$
ORC turbine	$\dot{W}_{turbine,\ ORC} = \dot{m}_{11} \times ((h_{11} - h_{12}) + (1 - y) \times (h_{12} - h_{13}))$
Evaporator 1	$Q_{Evaporator1} = \dot{m}_6 \times (h_7 - h_6)$
Condenser 1	$Q_{Condenser1} = \dot{m}_8 \times (h_8 - h_9)$
Evaporator 2	$Q_{Evaporator2} = \dot{m}_{10} \times (h_{11} - h_{10})$
Condenser 2	$Q_{Condenser2} = \dot{m}_{14} \times (h_{14} - h_{15})$

Energy has a significant impact on the ability of industries to produce, type of tools, and machines, methods of operation and transportation. Today, mankind has become so dependent on energy that it rarely even bothers to think about its role and impact, for this reason, researchers pay attention to improving the performance of energy production systems by trying to increase efficiency and reduce system costs. has been drawn.

As the driving force for production purposes, energy is considered the fundamental infrastructure of the social and economic activities of every country. The depletion of fossil fuels and environmental pollution problems have prompted policymakers to discover suitable and sustainable approaches for solving energy intricacies [1]. Researchers have endeavored to design and implement renewable energy systems such as geothermal energy and solar energy. As clean and renewable energy is inherent to the Earth, geothermal energy has been commercially used since 1913 [2], and its utilization in both electricity generation [3] and direct use [4] has grown rapidly over the last half-century. For example, only a small fraction of geothermal resources has been exploited so far [5]. With advancements in geothermal exploitation technologies and the

Table 3
Exergy destruction of system components.

System components	Relation
Evaporator 1	$\dot{E}_{Eva\,1} = \dot{E}_2 + \dot{E}_6 - \dot{E}_7 - \dot{E}_3$
Evaporator 2	$\dot{E}_{Eva\,2} = \dot{E}_3 + \dot{E}_{10} - \dot{E}_{11} - \dot{E}_4$
ORC turbine	$\dot{E}_{Turbine,\,ORC} = \dot{E}_{11} - \dot{E}_{12} - \dot{W}_{turbine}$
SRC turbine	$\dot{E}_{Turbine,\,steam} = \dot{E}_7 - \dot{E}_8 - \dot{W}_{turbine,\,steam}$
Condenser 1	$\dot{E}_{cond2} = \dot{E}_8 + \dot{E}_{31} - \dot{E}_9 - \dot{E}_{32}$
Condenser 2	$\dot{E}_{cond2} = \dot{E}_{14} + \dot{E}_{19} - \dot{E}_{15} - \dot{E}_{20}$
OFOH	$\dot{E}_{OFOH} = \dot{E}_{12} + \dot{E}_{17} - \dot{E}_{18}$
Pump No. 1	$\dot{E}_{pump1} = \dot{E}_9 + \dot{W}_{pump1} - \dot{E}_6$
Pump No. 2	$\dot{E}_{pump2} = \dot{E}_{15} + \dot{W}_{pump2} - \dot{E}_{16}$
Pump No. 3	$\dot{E}_{pump3} = \dot{E}_{18} - \dot{E}_{10}$
IHE	$\dot{E}_{IHE} = \dot{E}_{13} + \dot{E}_{16} - \dot{E}_{14} - \dot{E}_{17}$
PTSC	$\dot{E}_{PTSC} = \dot{E}_{sun} + \dot{E}_1 - \dot{E}_2 - \dot{E}_{17}$

Table 4
Purchase equipment cost of system components.

Component	Purchase equipment cost (Z_K)
PTC	$Z_{PTC} = 240 \times A_{ap\_tot}$
ORC turbine	$Z_{Turbine\ ORC} = 4750 \times \left(\left(\dot{W}_{turbine}^{0.75}\right) + 60 \times \left(\dot{W}_{turbine}^{0.95}\right)\right)$
SRC turbine	$Z_{Turbine\ steam} = 6000 \times \left(\dot{W}_{turbine}^{0.7}\right)$
Absorption chiller	$Z_{chiller} = 1144.3 \times \left(Q_{turbine}^{0.67}\right)$
Pump No. 1	$Z_{Pump1} = 3541 \times \left(\dot{W}_{Pump1}^{0.71}\right)$
Pump No. 2	$Z_{Pump2} = 3500 \times \left(\dot{W}_{Pump2}^{0.41}\right)$
Pump No. 3	$Z_{Pump3} = 3500 \times \left(\dot{W}_{Pump3}^{0.41}\right)$
Condenser 1	$Z_{Cond1} = 150 \times \left(A_{Cond1}^{0.8}\right)$
Condenser 2	$Z_{Cond2} = 150 \times \left(A_{Cond2}^{0.8}\right)$
Evaporator 1	$Z_{Evap\ 1} = 276 \times \left(A_{Evap\ 1}^{0.88}\right)$
Evaporator 2	$Z_{Evap2} = 276 \times \left(A_{Evap2}^{0.88}\right)$
PEM electrolyzer	$Z_{electrolyzer} = 1000 \times W_{PEM}$
RO desalination unit	$Z_{RO} = 1000 \times \dot{m}_{28} \times 0.98$

Table 5
Cost balance and axillary relations for system components [43,47–49].

Component	Cost balance	Auxiliary equation
PTC field	$\dot{C}_{sun} + \dot{C}_1 + \dot{Z}_{solar} = \dot{C}_2$	$c_1 = c_2\,,\ c_{sun} = 0$
SRC turbine	$\dot{C}_7 + \dot{Z}_{Steam,T} = \dot{C}_8 + \dot{C}_{Steam,T}$	$c_7 = c_8$
ORC turbine	$\dot{C}_{11} + \dot{Z}_{ORC,T} = \dot{C}_{12} + \dot{C}_{13} + \dot{C}_{ORC,T}$	$c_{11} = c_{12}\,,\ c_{11} = c_{13}$
Condenser 1	$\dot{C}_8 + \dot{C}_{31} + \dot{Z}_{Con1} = \dot{C}_9 + \dot{C}_{32}$	$c_8 = c_9, c_{31} = 0$
Condenser 2	$\dot{C}_{14} + \dot{C}_{19} + \dot{Z}_{cond} = \dot{C}_{15} + \dot{C}_{20}$	$c_{14} = c_{15}\,,\ c_{19} = 0$
Evaporator 1	$\dot{C}_2 + \dot{C}_6 + \dot{Z}_{Eva1} = \dot{C}_3 + \dot{C}_7$	$c_2 = c_3$
Evaporator 2	$\dot{C}_3 + \dot{C}_{10} + \dot{Z}_{Eva2} = \dot{C}_4 + \dot{C}_{11}$	$c_3 = c_4$
Pump 1	$\dot{C}_9 + \dot{C}_{P1} + \dot{Z}_{Pump1} = \dot{C}_6$	$c_{P1} = c_{Steam,T}$
Pump 2	$\dot{C}_{15} + \dot{C}_{P2} + \dot{Z}_{Pump2} = \dot{C}_{16}$	$c_{P2} = c_{ORC,T}$
Pump 3	$\dot{C}_{18} + \dot{C}_{P3} + \dot{Z}_{Pump3} = \dot{C}_{10}$	$c_{P3} = c_{ORC,T}$
IHE	$\dot{C}_{13} + \dot{C}_{16} = \dot{C}_{14} + \dot{C}_{17}$	$\dot{C}_{13} = \dot{C}_{14}$
OFOH	$\dot{C}_{12} + \dot{C}_{17} = \dot{C}_{18}$	–
PEM electrolyzer	$\dot{C}_{32/} + \dot{C}_{PEM} + \dot{Z}_{PEM} = \dot{C}_{33} + \dot{C}_{35}$	$\dot{C}_{33} = \dot{C}_{35}$
RO desalination unit	$\dot{C}_{36} + \dot{Z}_{RO} = \dot{C}_{39} + \dot{C}_{38}$	$\dot{C}_{39} = \dot{C}_{38}, \dot{C}_{36} = 0$
Absorption chiller	$\dot{C}_4 + \dot{Z}_{chiller} = \dot{C}_5 + \dot{C}_{chiller} \times Q_e$	$c_4 = c_5$

demand for renewable and low-carbon-producing energy, there is a high prospect for the accelerated use of geothermal energy in the future. However, its scope of application is limited because of the limited temperature achieved by geothermal energy. Therefore, a hybrid application should be implemented to further enhance the temperature by integrating geothermal energy with other forms of renewable energy, such as concentrated solar-thermal technology [6,7]. Solar energy is regarded as the most promising material for wide utilization, and

Table 6
Validation of the RO desalination unit.

Variable	Unit	Present Study	Nafey [105]	Difference (%)
$\dot{W}_{pump\_RO}$	kW	1122	1131	0.796
M_f	m^3/h	485.9	485.9	0
S_R	–	0.9944	0.9944	0
X_b	ppm	64,180	64,180	0
X_d	ppm	252	250	0.8
ΔP	kPa	6856	6850	0.088

concentrated solar-thermal technology is one of the dominant solar utilization applications; the technology can make the heat transfer fluid (HTF) inside heat-collection elements achieve high-grade thermal energy at high temperatures [8,9]. A commercial parabolic trough solar collector (PTSC), as a popular concentrated solar-thermal technology, can harvest the thermal energy of HTFs at almost 400 °C [10,11]. The high-temperature thermal energy obtained can be adopted in cascade utilization systems according to the residual energy grades. For instance, high-grade thermal energy can first be carried to thermal-power systems based on the Steam Rankine cycle [12] and the ORC [13]; then, the residual low-grade thermal energy can continue to be used in other systems, such as absorption cooling systems [14]. Many researchers have been conducting tremendous efforts in the research and development of geothermal energy, concentrated solar-thermal technology, and hybrid renewable systems. In the field of integrated geothermal energy applications, Heidarnejad et al. [15] attempted to optimize a geothermal site using biomass to generate power and freshwater. Kahraman et al. [16] thermodynamically analyzed a geothermal power plant using air conditioning and investigated the effect of ambient temperature change on the plant's efficiency. Kianfard et al. [17] analyzed a freshwater- and hydrogen-producing geothermal-driven system from economic and exergy standpoints. Alirahmi et al. [18] studied a fuel cell-electrolyzer combination for the load management of the network peak in a geothermal site to convert power to hydrogen and vice versa. In the field of PTSC-integrated applications, Hu et al. [19] optimized a combined geothermal-solar energy system thermally and economically. Kerme et al. [20] analyzed a multigenerational system based on solar energy utilization. In this study, the required energy of the system was supplied by the PTSC's absorption of thermal energy from the sun. The results revealed that the solar collector and reverse osmosis (RO) desalination unit were the main sources of exergy destruction. Assareh et al. [21] probed a renewable system based on solar and geothermal energy usage, fueled by thermoelectric generators to produce power, cooling, and freshwater. Their findings indicated that the replacement of a thermoelectric generator with a condenser reduced the total cost rate and exergy efficiency of the enhanced system. Kumar Gupta et al. [22] designed a renewable system that included an ORC with a triple-pressure level vapor absorption system and a PTSC solar system. The system concurrently generates cooling and energy at two different working temperatures. Assareh et al. [23,24] conducted energy, exergy, multi-objective optimization, and economic analysis on a multi-generation system, producing solar-based power, hydrogen, freshwater, cooling, and heating in Dezful. Furthermore, a PEM electrolyzer was designed to supply the network-required power in addition to the load at different times.Through the above state-of-the-art research on multi-generation systems involving geothermal energy and PTSC, note that the selection of HTF in PTSCs has been the focus of published literature because it is directly associated with its ability to absorb and convey thermal energy. Bellos et al. [25] reviewed the heat transfer fluids, namely, Therminol VP1, sodium liquid, molten salt, CO_2, air, Helium, and water for use in PTSCs. They reported that, for extremely high temperatures, helium, and CO_2 were the most suitable heat transfer fluids, and the sodium liquid achieved the highest exergetic efficiency of 47.48% at 800 K. Dehaj et al. [26] experimentally assessed the use of nickel ferrite ($NiFe_2O_4$) nanofluids in a PTSC. They asserted that the

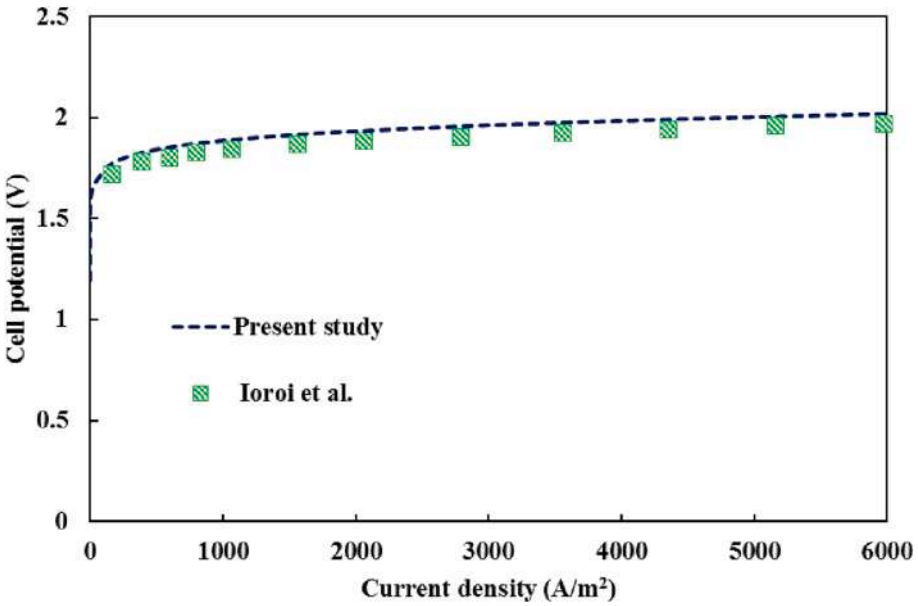

Fig. 2. Validating the PEM electrolyzer of the proposed system [106].

Table 7
Electrolyzer PEM information.

Property	Value
MW	Molar mass (Hydrogen)
T_{Ele}	80 [c]
F	96,487 [C/mol]
D	$50*10^{-6}$ [m]
$lambda_a$	14
$lambda_c$	10
J	500 [A/m^2]

thermal efficiency of the PTSC was enhanced by the volume fraction and flow rate of the nanofluid. Further, a 51% maximum efficiency was achieved at 0.05% volume fraction and 3 L/min flow rate. Malekan et al. [27] modeled the heat transfer in PTSCs with Fe_3O_4 and CuO/Therminol 66 heat transfer fluids. They stated that the collector efficiency was higher when Fe_3O_4 was employed, and the increase in volume fraction and decrease in particle size enhanced it. Malviya et al. [28] comprehensively evaluated different heat transfer fluids in PTSC applications. The effect of the heat transfer fluid on tube-absorber material was studied. The effects of the outer temperature level, exergy efficiency, and tube-absorber material were investigated. They asserted that Therminol VP1 and water were the best choices for the heat transfer fluid at high and low temperatures respectively. Interestingly, air should not be used in any temperature range. In addition, other very useful articles [29–33] can be reviewed to gain a better understanding of this article's proposed system. Examining these studies helps to understand the innovation of the present work.Many studies have been conducted in the field of using renewable energies, especially the available solar energy, as well as other renewable energies such as fuel cells, geothermal, etc. And sunlight has been made, which can be used in new and clean systems [34–53].

Also, the issue of reducing the emission of environmental pollution and, on the other hand, meeting the consumption needs of residential buildings and industrial centers from clean energy has been taken into consideration, which requires many studies to be able to introduce this clean science to start it with high performance [54–71].

In 2020, Cuceet al. worked to improve the thermal performance of thermoelectric coolers (TEC) by designing a nanofluid-driven water-to-air heat exchanger. Three different nanoparticles (Al2O3, TiO2, and SiO2) with mass fractions of 0.1, 0.5, and 1% were added to the running water in the system and the temperature difference between the first and final states of the cooling process was determined for different ambient temperatures. The results showed that despite the slight decrease in the coefficient of performance (COP) values of the system, it can be easily claimed that the new TEC design integrated with nanofluids and water-to-air heat exchanger block is much more beneficial than conventional water cooling units [72].

In 2022, Mert Cuce et al. investigated the effect of using hybrid nanofluids as a coolant on the thermal performance of portable thermoelectric refrigerators. Hybrid nanofluids prepared with Al2O3-TiO2-SiO2 and nanoparticles and water were used as refrigerants in the system. To evaluate the thermal performance of these hybrid nanofluids, the experiments were repeated using water without added nanoparticles as a reference case. According to the results obtained from the experimental study, it was observed that in all cases, the experiments using nanofluids had better results than the reference cases. In addition, it was found that the efficiency obtained from the system increases in all cases as the ratio of nanoparticles in the mixture increases [73].

In 2023, Shakibi et al investigated a system based on solar energy and natural gas to produce freshwater. The proposed system consisted of a heliostat field with a gas turbine cycle, multi-effect desalination, steam Rankine cycle, organic Rankine cycle, and thermoelectric generator. To optimize the system, a combined model of support vector regression,

Table 8
Heat transfer fluid properties.

Heat transfer fluid	Density (kg/m^3)	Kinematic viscosity cSt (mm^2.s)	Specific heat capacity (kJ/kg.K)	Thermal conductivity (W/m.K)	Operating range (°C)	Flash point (°C)
Therminol 59	974	7.04	1.68	0.1213	−49 to 315	146
Marlotherm SH	1040	16	1.56	0.1305	−5 to 350	219
Syltherm 800	936	10	1.608	0.1350	−40 to 400	160
Therminol VP1	1064	4.03	1.546	0.1363	12 to 400	124

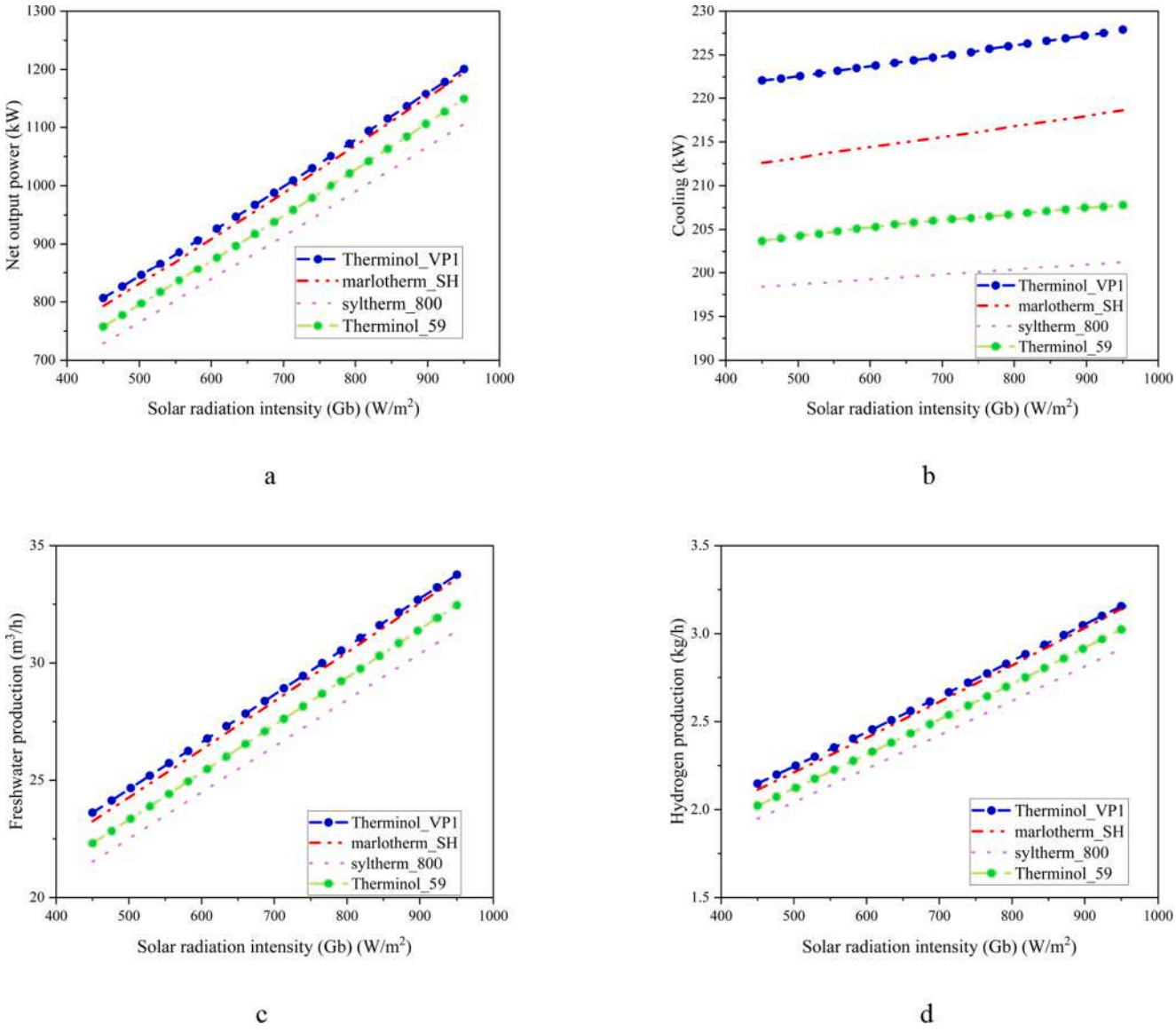

Fig. 3. Effect of solar radiation intensity (G_b) on system outputs (with different heat transfer fluids): **(a)** power, **(b)** cooling production, **(c)** freshwater, **(d)** hydrogen production, **(e)** exergy efficiency, **(f)** energy efficiency, **(g)** cost rate, and **(h)** levelized cost.

multi-objective gray wolf optimization algorithm, multi-objective grasshopper optimization algorithm, and two different decision-making methods were proposed. According to the obtained results, exergy efficiency, total product cost rate, and CO_2 emission were reported as 45.6%, 2.716 dollars/gJ, and 30.26 kg/s of freshwater respectively. Furthermore, after system optimization, the total exergy destruction rate decreased from 15,153 kW to 14,820 kW [74].

In 2023, Shakibi et al. conducted an economic study and multi-objective optimization of a solar and wind power plant and conducted a case study to determine the performance of the system to the climate changes of the city of Las Vegas. The investigated multiple generation system including parabolic solar collector, wind turbine, thermoelectric generator, and its combination with steam Rankine cycle was suggested to produce higher electricity. Also, a reverse osmosis desalination unit and a single effect absorption chiller and proton exchange membrane electrolysis were used to produce freshwater and hydrogen production cooling. A case study that considered the conditions of the city of Las Vegas produced 22.02 megawatt hours of power and 4.50 tons of carbon dioxide in one year, resulting in an environmental cost of $107.8 per year [75].

In 2023, Assraeh et al. investigated a renewable system based on solar energy to produce electricity and freshwater from a new gas power plant and a solar power plant and conducted a case study of climate changes in Australia, Spain, South Korea, and Iran. They gave. In this study, a new power plant configuration consisting of a concentrated solar power plant integrated into a Brayton cycle before the combustion chamber was investigated. Among the most importantly effective and practical parameters in this research, we should mention gas turbine efficiency, inlet temperature to the organic turbine, inlet pressure to the steam turbine, and inlet temperature to the gas turbine [76].

In 2022, Assraeh et al. worked on thermodynamic modeling and economic evaluation of a cogeneration system of power and freshwater based on compressed air energy storage and multi-effect desalination. This study examines the design of a renewable system for generating electricity and freshwater based on the solar cycle and the use of thermal storage in different cities. The results showed that the parameters of the number of heliostats and turbine and compressor efficiency have the greatest effect on the system outputs. Based on the economic analysis of the system, the costs of the compressed air storage source, the solar unit, and the gas turbine were the highest among the costs of the system components [77].

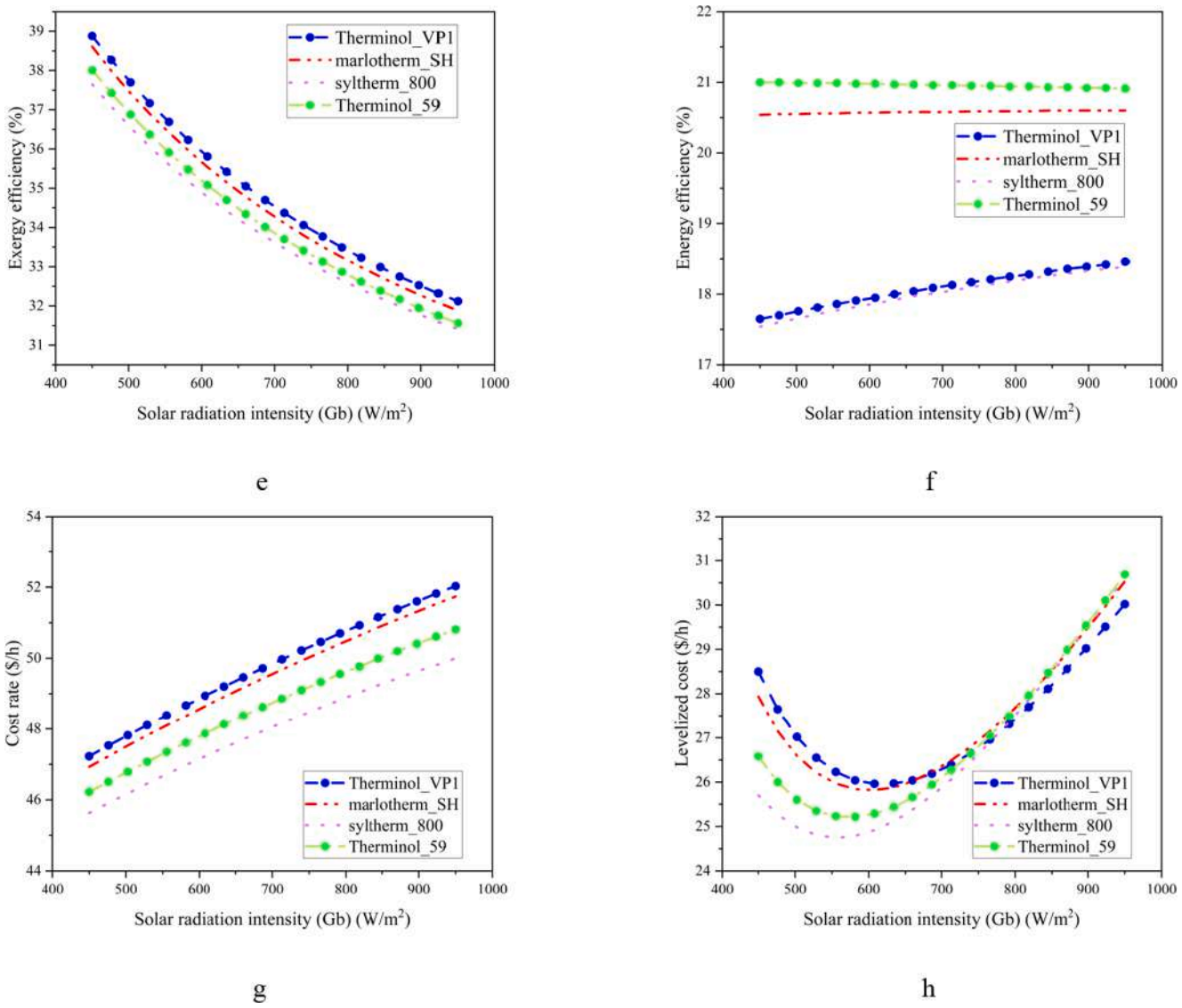

Fig. 3. (*continued*).

In 2023, Dezhdar et al used solar energy and ocean thermal energy to supply the required energy for a power generation system. This system was launched based on the use of the temperature difference of the dam water and the absorption of solar radiation energy in that area. A case study was conducted on climate changes at Karkheh Andimeshk Dam in Iran, and the system consisted of two solar units and an organic Rankine cycle, and a thermoelectric generator was used to increase the performance of the system in electricity generation [78].

In 2023, Pourmoghadam and Kassaiyan used the energy-economic evaluation of multiple production systems based on solar energy and the use of parabolic collectors to feed from the sun to produce cooling, heating, electricity, and water. Their proposed system was modeled with the help of Mattel, solving engineering equations and TRNSYS software. The results showed that toluene organic fluid has the best annual performance for power generation. Also, the repayment period for the base case was determined to be 6 years [79].

In 2022, Karaca et al. investigated the development of an integrated solar and wind energy system for desalination and power generation, specifically for Antigua and Barbuda, an island nation in the Caribbean Sea, to reduce the region's reliance on energy infrastructure. Based on volatile fossil fuels and reduce pollution. The evaluation of the system showed that the system is functional with energy and exergy efficiency of 45.4% and 37.6%, respectively. The annual electricity production of this system was estimated to be 316 GW-hours, equivalent to 102.6% of the annual electricity needs of Antigua and Barbuda. In addition, the system supplies 124 tons of freshwater and compressed air per day to fuel 140 short-range (80 km) wind cars. Environmental analysis showed that the implementation of the potential system can reduce the emission of greenhouse gases in the region by 88% [80].

In 2022, Razmi et al reported the concept of green hydrogen energy storage based on a parabolic collector and proton exchange membrane electrolyzer/fuel cell by thermodynamic and exerguaeconomic analyses with multi-objective optimization. The main goal of this research is to introduce a new configuration of green hydrogen production for electricity generation in periods of peak demand and an innovative hybridization of a solar unit based on a parabolic collector with a proton exchange membrane electrolysis and a fuel cell from a thermodynamic and exergoeconomic point of view became. A sensitivity analysis and a multi-objective optimization based on a combination of neural network and gray wolf optimization algorithms were performed to select the best working fluid for the solar unit and the ideal operating conditions according to the minimum cost rate and maximum exergy efficiency. The results showed that the proposed system can generate 9, 14.9, and 20.1 MW of electricity in off-peak, middle, and peak times, respectively. Also,

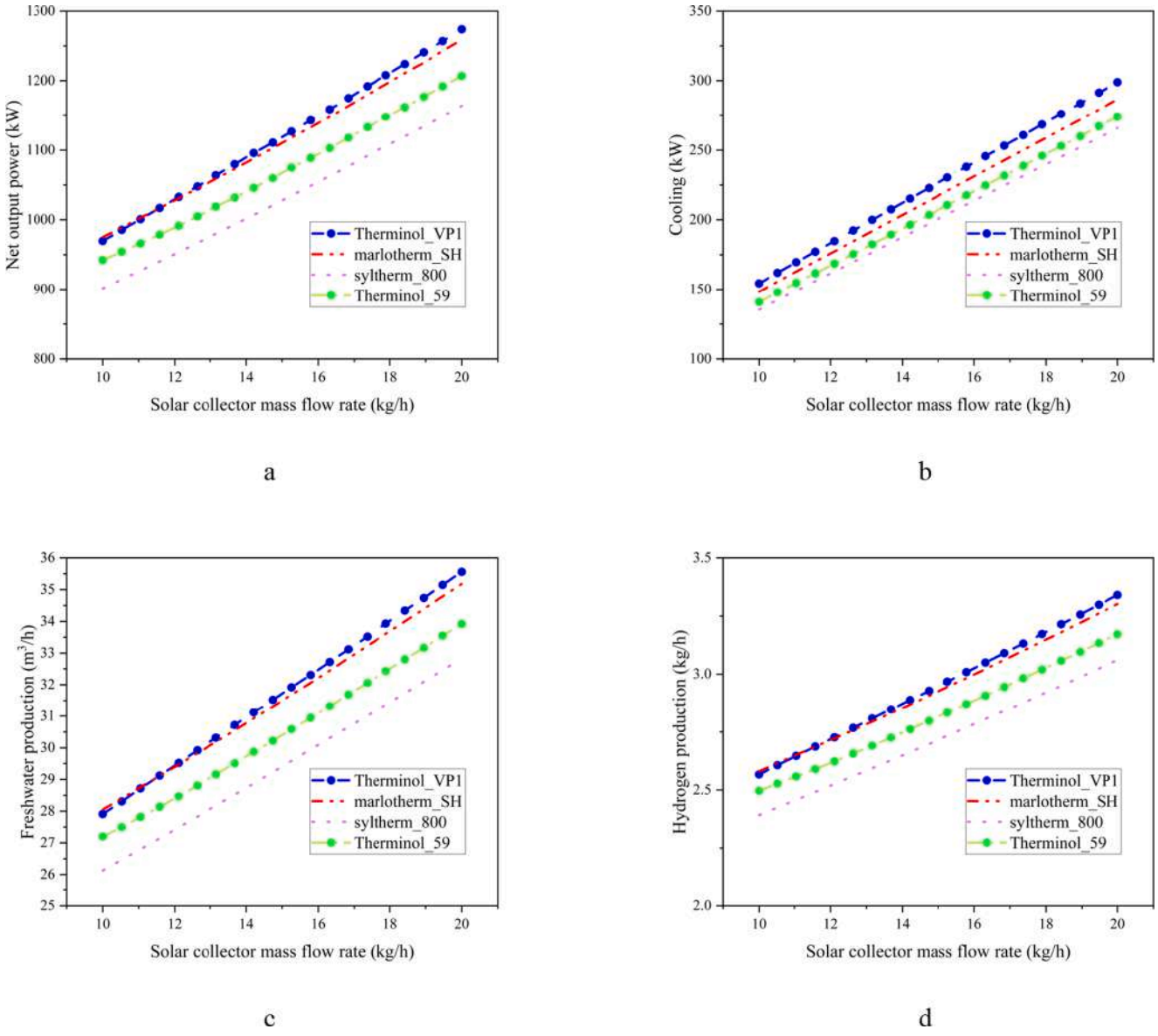

Fig. 4. Effect of the solar collector mass flow rate on system outputs (with different heat transfer fluids): **(a)** net output power, **(b)** cooling production, **(c)** freshwater production, **(d)** hydrogen production, **(e)** exergy efficiency, **(f)** energy efficiency, **(g)** cost rate, and **(h)** levelized cost.

the results showed that the proposed system works with an exergy efficiency of 17.6% and a cost rate of $492.4 per hour under optimal conditions [81].

Also, in 2022, Rajeb et al. investigated an innovative integrated multi-generation solar energy system for the production of hydrogen, oxygen, electricity, and green heat. The designed system includes photovoltaic solar thermal collectors (PVT) with organic Rankine cycle (ORC), PEM electrolyzer, and liquid natural gas. Using engineering equation solving (EES), thermodynamics (energy, exergy), and economic evaluation of the proposed power plant were done. Non-dominated sorting genetic algorithm was used to estimate the optimal results for the proposed system. The objective functions are energy efficiency, cost rate, and net power output. The results showed that the proposed system operates with an exergy efficiency of 16.24%, a cost rate of $4.48/hour, and a net electrical power of 33.32 kW under optimal conditions, based on TOPSIS (Technique for Similarity-Based Order Performance) [82].

In 2022, Nedai et al. evaluated the performance of multiple production systems based on solar energy absorption based on the heliostat field and using Brayton's closed cycle, absorption refrigeration cycle, desalination and dehumidification and proton exchange membrane electrolysis along with multi-objective optimization they paid. The results showed that the simulation in basic operational conditions has resulted in the production of 8.32 MW of power, 3.16 kg/s of freshwater, 8.37 MW of cooling load, and 0.22 kg/h of hydrogen with an exergy efficiency of 39.15% and $8.81/gizole [83].

Today, meeting energy needs with the least environmental impact is a serious challenge that must be solved with knowledge and technology. Therefore, the development of energy systems to produce electricity with high performance and reduce CO_2 emissions as well as the reasonable cost is of great importance. In this regard, in this research, a system for producing clean electricity is proposed to deal with this issue.

The present study proposes a polygene-ration power plant combining solar and geothermal energies with a steam Rankine cycle (SRC) and ORC, an absorber chiller, an RO desalination unit, and PEM electrolyzer subsystems, which produce electricity, cooling, freshwater, and hydrogen. The study focuses on selecting a suitable heat transfer fluid for the PTSCs. Thermodynamic and economic analyses were applied, and multi-objective optimization was implemented. Additionally, the system was configured for use in Bandar Abbas as a case study. The goal

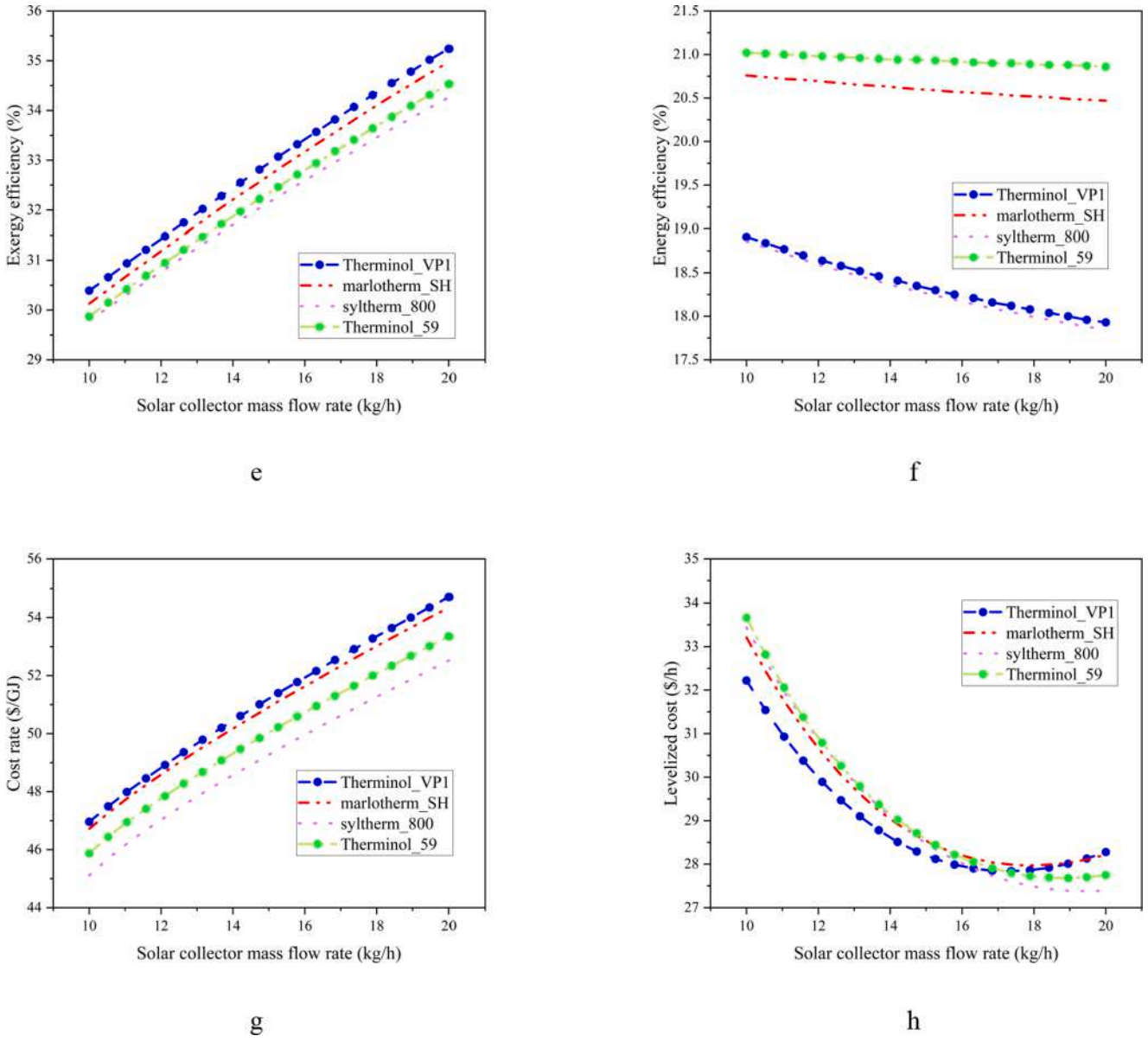

Fig. 4. (*continued*).

and innovation of this study are to produce clean products with the proposed system. Engineering Equation Solving (EES) software is used to model and obtain thermodynamic software results. Finally, in the proposed system with the optimum HTF, an efficient optimization procedure based on an artificial neural network (ANN) and NSGA-II optimizer is implemented.

The innovations of this research can be stated as follows:

- Simultaneous use of two renewable solar and geothermal energies with high potential and high availability.
- Using energy, exergy, and exergeoeconomic analyses to provide a comprehensive view of system performance and capabilities.
- The combination of two power generation units including the steam Rankine cycle and the modified organic Rankine cycle.
- Providing a multiple energy production system including four products: electricity, cooling, hydrogen, and freshwater.
- Reviewing different lubricants for parabolic solar collectors and introducing the best lubrication.
- From the thermoelectric generator to increase the electricity produced by the system
- Analyzing Sankey to calculate the amount of exergy and exergy destruction of units and system equipment.
- Feasibility of starting the proposed system in Bandar Abbas city in Iran.
- Optimization of the investigated objective functions with two neural network methods and the use of the genetic algorithm.

2. System description

Fig. 1 depicts the schematic of the proposed polygene ration system. This system, grounded on geothermal and solar energies, comprises several subsystems, including PTSCs, SRC, ORC, PEM electrolyzer, LiBr absorption chiller, and RO desalination units. The system generated electricity, hydrogen, cooling, and freshwater. The geothermal output fluid with a temperature of 160–190 °C directly entered the PTSC, and by exchanging heat with the heat transfer fluid of the PTSC, its temperature increased to 340 °C. After the solar collector, the geothermal fluid transfers its heat to the SRC, ORC, and absorber chiller and is injected back into the reinjection wells. Water is used for the SRC condenser in this system, the output of which is divided into two parts:

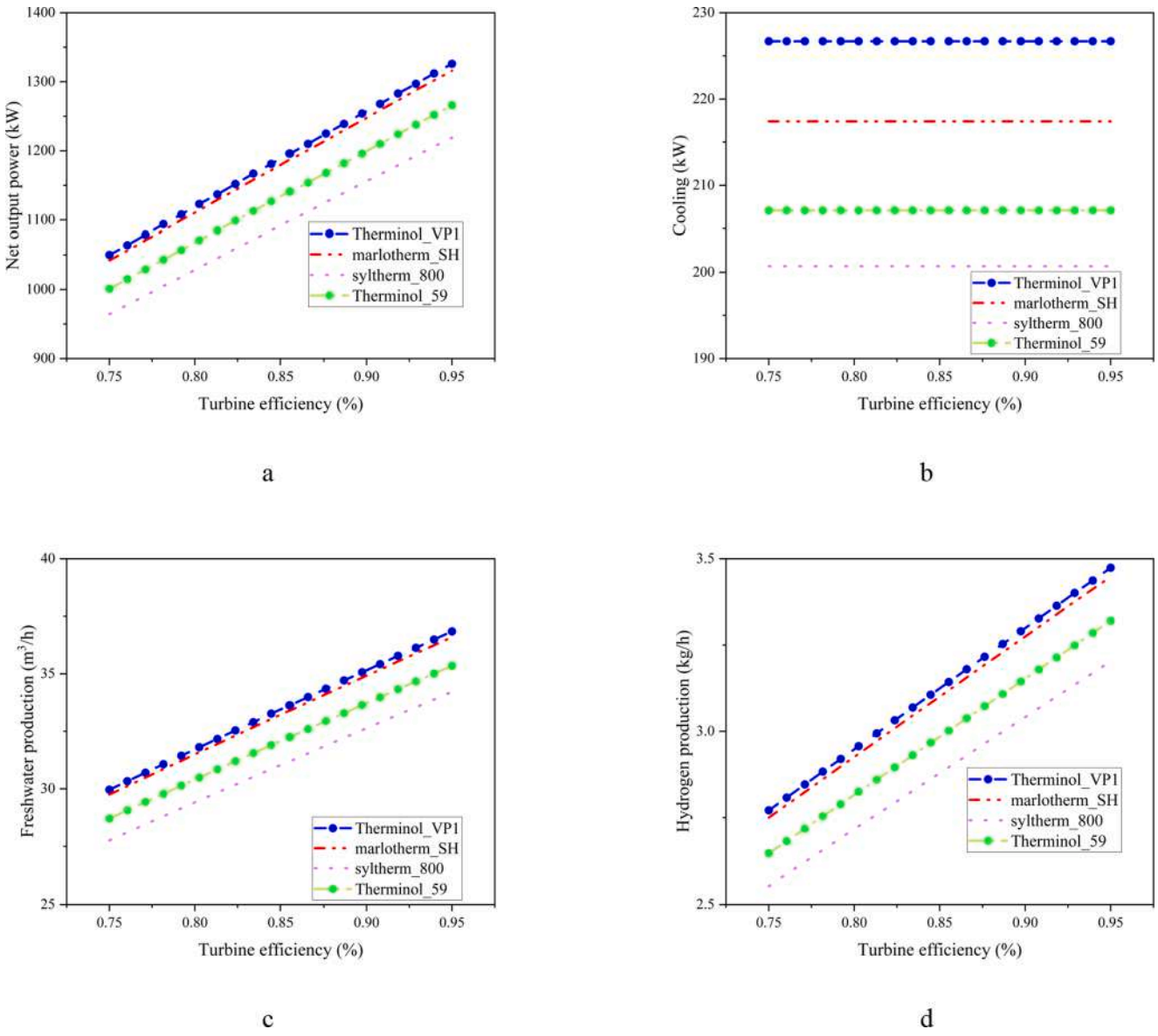

Fig. 5. Effect of turbine efficiency on system outputs (with different heat transfer fluids): **(a)** net output power, **(b)** cooling production, **(c)** freshwater production, **(d)** hydrogen production, **(e)** exergy efficiency, **(f)** energy efficiency, **(g)** cost rate, and **(h)** levelized cost.

hot water (stream 32) for domestic consumption and hot water required by the electrolyzer. The efficiency of the evaporator depends on the fluid type, tube surface, material, temperature difference, and other factors. The R123 refrigerant is the working fluid used in the ORC that enters the ORC turbine (stream 11), produces power similar to SRC, and passes an open feed-water organic heater (OFOH) and internal heat exchanger (IHE). In the organic Rankine cycle, an internal heat exchanger and open feedwater heater are used to improve the efficiency of the Rankine cycle and enhance its power generation. Saturated steam with a quality of one exits the evaporator (stream 7), proceeds to the SRC turbine, and supplies power that can be used in the electrolyzer and RO desalination unit. A share of the generated power is delivered to the power distribution network. In the PEM electrolyzer, water is fed, and power is supplied by the SRC and ORC turbine, eventually producing hydrogen (stream 33). The geothermal fluid (stream 4) exchanges heat with the generator of the LiBr absorption chiller, and cooling is produced. Finally, seawater (stream 35) enters the RO desalination unit and is converted to freshwater (stream 37).

The main goal of this research is to introduce a multiple energy production system based on the use of two high-potential renewable energies for all regions and countries of the world, including solar and geothermal energies, using a parabolic-linear solar collector and using two cycles. The modified organic Rankine and steam Rankine cycle in the system along with the use of absorption chiller, reverse osmosis, and PEM electrolyzer produce useful products needed by humans including freshwater, hydrogen, cooling, and electric energy.

To model the system and obtain the results of the parametric analysis of the system, thermodynamic software for solving engineering equations (EES) was used. To optimize the designed system, the multi-objective genetic sorting algorithm (NSGA-II) was used to find the best value for the objective functions. The two conflicting objective functions investigated include increasing exergy efficiency and decreasing cost. The advantages of this system include high energy utilization, reduction of energy losses and exergy, high efficiency of exergy, and reduction of greenhouse effects.

3. Methodology

The proposed polygene ration system was modeled in the EES software environment using the input data presented in Table 1.

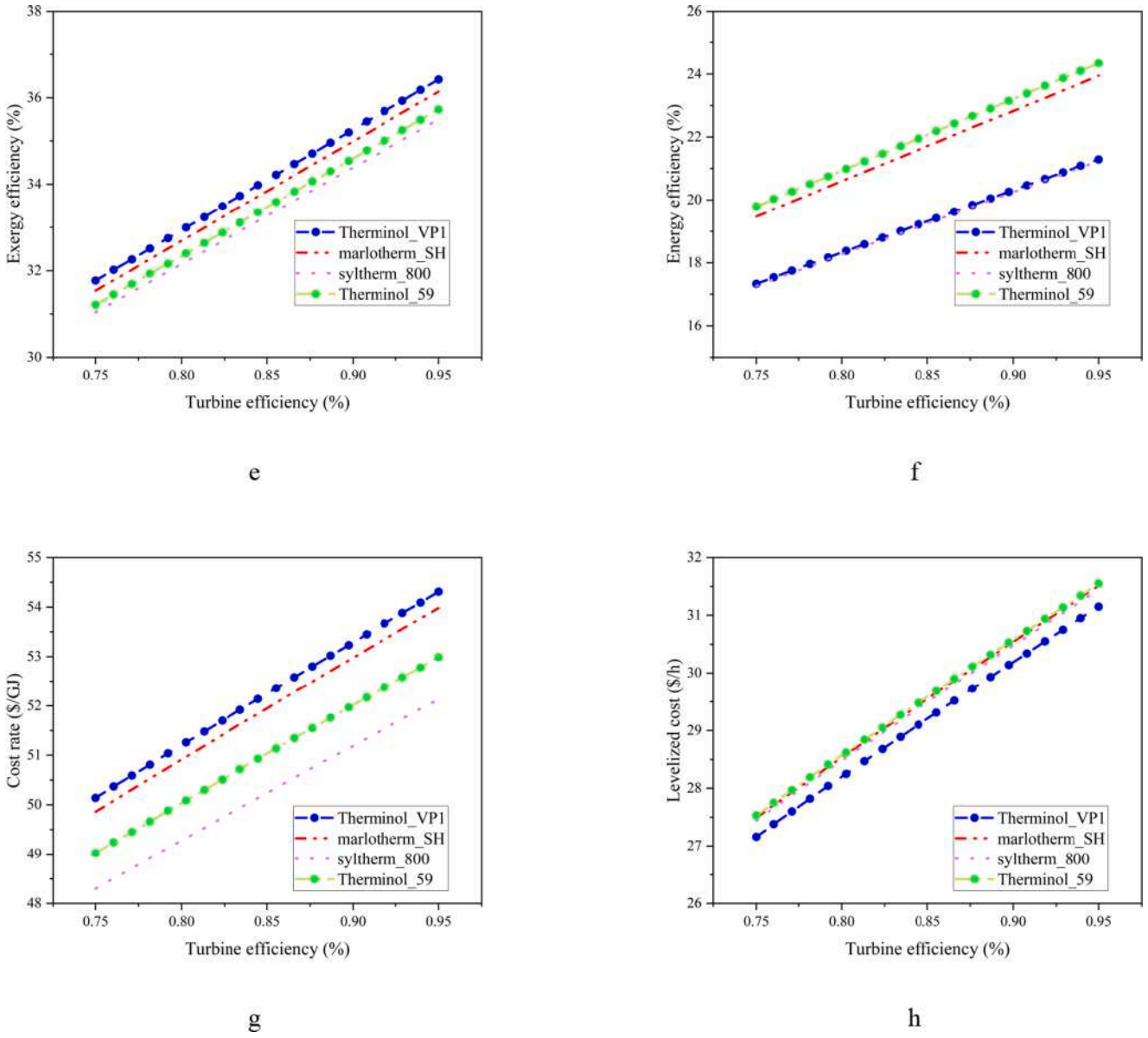

Fig. 5. (*continued*).

As mentioned earlier, this system uses two renewable energies, geothermal and solar, so after the parameters affecting this system, we can mention the intensity of solar radiation and the mass flow rate entering the collector. Because the activity of the system can increase or decrease by absorbing solar energy. In other words, on the hot days of the year and in the hottest hours of the day when solar radiation increases, the performance of the system also increases, because the thermal energy absorbed by the system increases. The input temperature from the geothermal source can also cause changes in the system performance, it should be noted that the three units of organic Rankine cycle, steam Rankine cycle, and absorption chiller work with thermal energy. So by supplying the required energy of these three units, it is possible to improve the overall performance of the system. Also, by changing the efficiency of the turbine and pump, you can see changes in the performance of the system. Other parameters include ambient temperature, ambient pressure, etc., which are part of the environmental and technical parameters of the system, according to studies in the field of research, it was concluded that they can influence the functional changes of the system.

3.1. Parabolic trough collectors (PTSC)

The following equations were used to calculate the rate of useful energy generation in the PTSCs [29–31]:

$$\dot{Q}_u = \dot{m}_1[C_{Pc} \times T_2 - C_{Pc} \times T_1] \quad (1)$$

$$\dot{Q}_u = n_{ptc}F_R[S \times A_{ap} - A_r \times U_L \times (T_1 - T_0)] \quad (2)$$

where T_1 and T_2 denote the output water temperatures at points 1 and 2, respectively; C_{pc} is the specific heat capacity at constant pressure; $\dot{m}$ is the mass flow rate of the collector; F_R is the heat removal factor; U_L is the collector's total pressure drop; A_{ap} is the collector's plate area; and S is the visual efficiency, computed using [21]:

$$S = G_b\eta_r \quad (3)$$

$$\eta_r = \rho_c \times \lambda \times \tau_c \times k_y \times \alpha \quad (4)$$

$$A_{ap} = (width - D_{co})^*Length \quad (5)$$

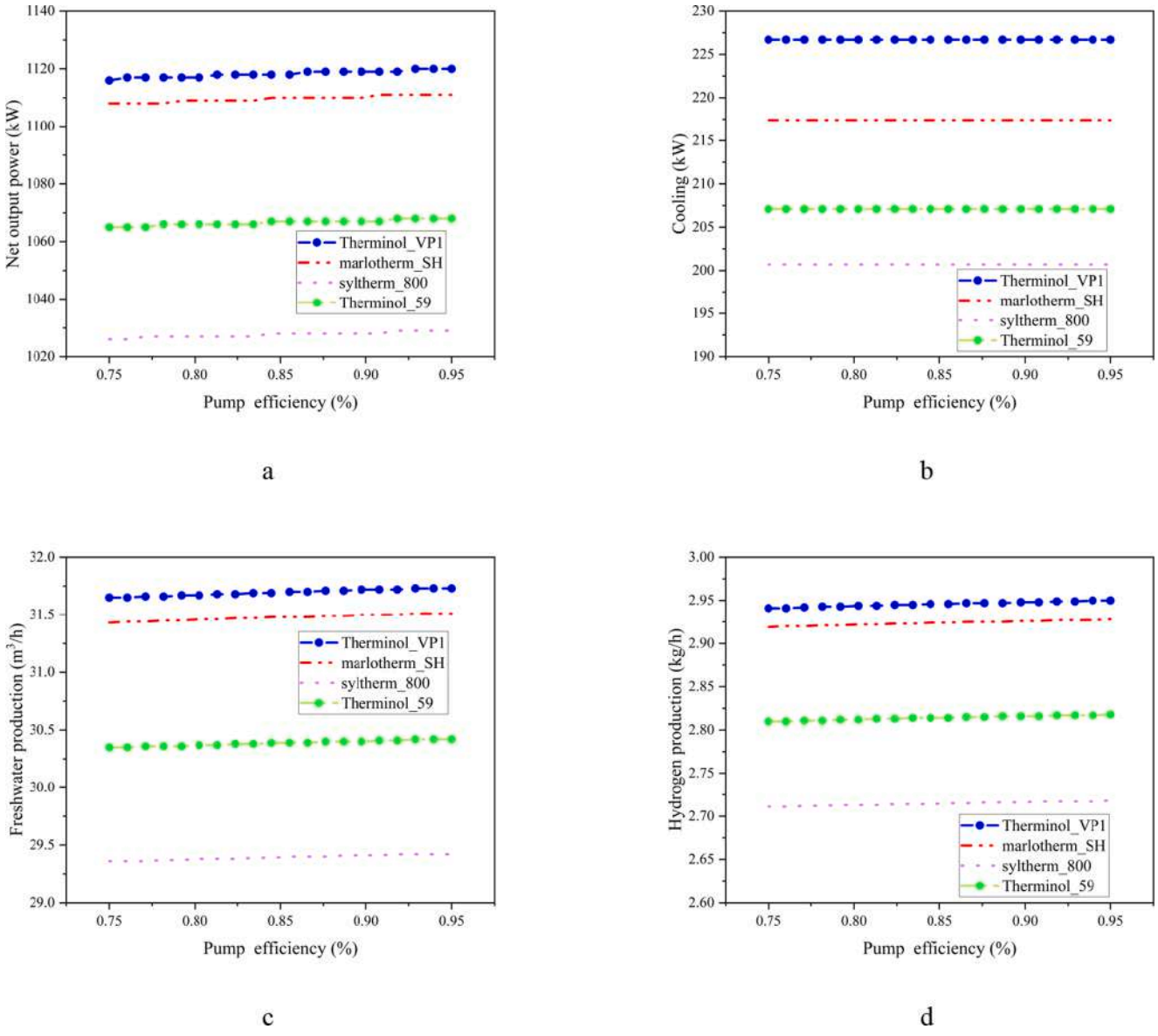

Fig. 6. Effect of pump efficiency on system outputs (with different heat transfer fluids): **(a)** net output power, **(b)** cooling production, **(c)** freshwater production, **(d)** hydrogen production, **(e)** exergy efficiency, **(f)** energy efficiency, **(g)** cost rate, and **(h)** levelized cost.

Here, G_b is the solar radiation intensity, η_r is the efficiency of the solar collector, ρ_c is the reflectance, τ_c is the transmittance of the cover glass, α is the absorptivity of the PTSC, λ is the interception factor, and F_R is determined by [84,85]:

$$F_R = \frac{\dot{m}_1 C_{p\_c}}{A_r U_L}\left[1 - exp\left(-\frac{A_r U_L F_1}{\dot{m}_1 C_{p\_c}}\right)\right] \tag{6}$$

$$F_1 = \frac{\frac{1}{U_L}}{\frac{1}{U_L} + \frac{D_{o\_r}}{h_{fi}} + \left(\frac{D_{o\_r}}{2k} ln \frac{D_{o\_r}}{D_{i\_r}}\right)} \tag{7}$$

where F_1 is the collector efficiency factor. The following equation was used to determine the area of the PTSCs [32]:

$$A_{p\_tot} = n_{ptc} \times A_{ap} \tag{8}$$

3.2. PEM electrolyzer

Electrolyzer is a device that splits water into hydrogen and oxygen using direct electric current. In other words, it is a means of converting electrical energy into chemical energy, which can be considered as a non-linear voltage-sensitive DC load. By increasing the DC voltage applied to the electrolyzer, its current increases, and more hydrogen is produced.

The SRC cycle turbine supplies the power required by the PEM electrolyzer for electrochemical reactions. After passing through the pump, seawater enters the PEM electrolyzer, where a hydrogen and water-oxygen mixture is produced. The following equations were used to model the PEM electrolyzer [17,86–93]. The power output of the PEM electrolyzer is calculated as follows:

$$\dot{W}_{\mathrm{PEM}} = 0.25 \times \dot{W}_{total} \tag{9}$$

The generated hydrogen rate is calculated using:

$$\dot{N}_{H2_{\mathrm{Out}}} = 3600 \times \dot{M}_{H2_{\mathrm{Out}}}\ \mathrm{kg/h} \tag{10}$$

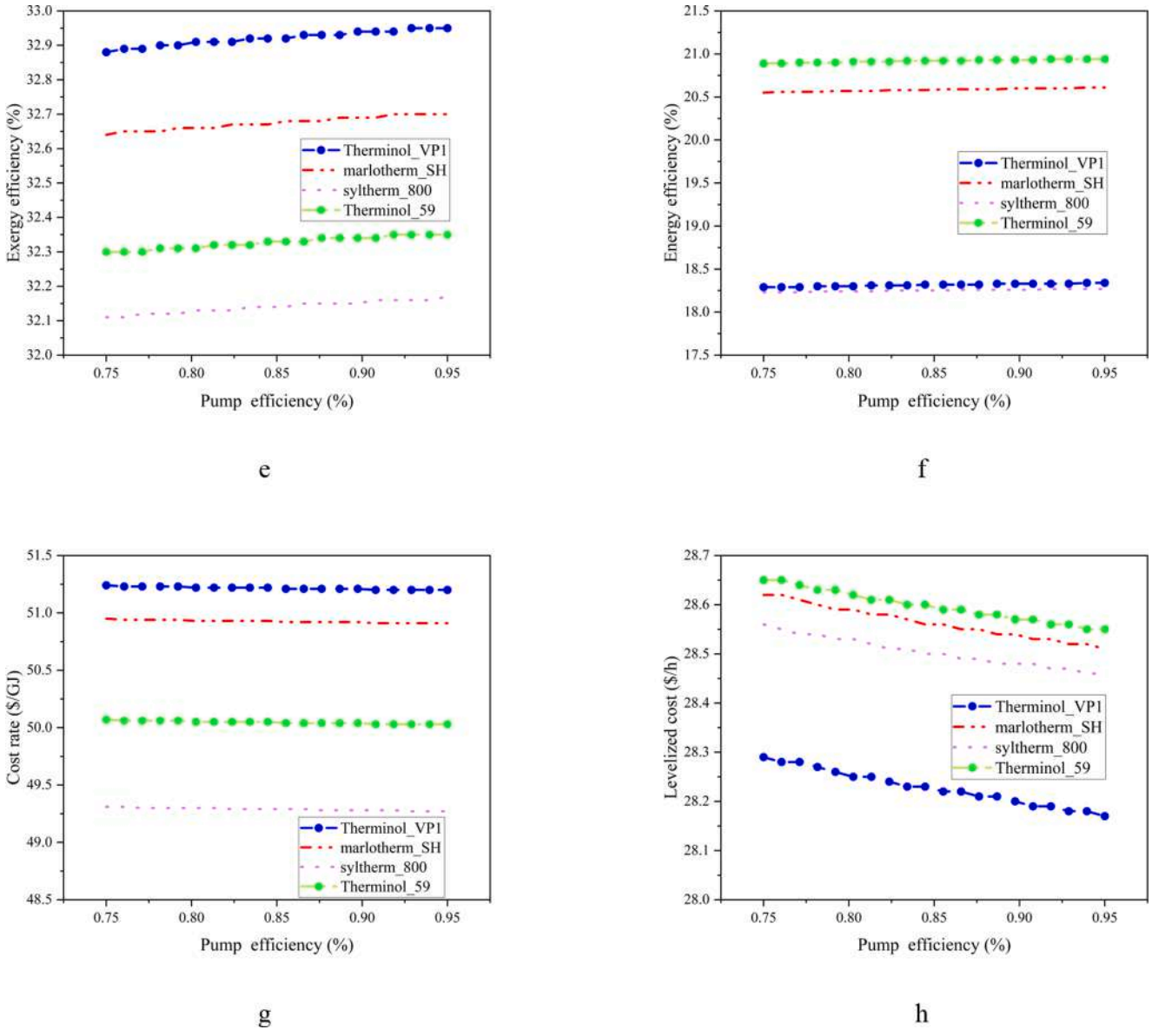

Fig. 6. (*continued*).

$$\dot{M}_{H2_{Out}} = a_{H2} \times \dot{W}_{PEM}^{\ b_{H2}} + c_{H2} \ \text{kg/s} \tag{11}$$

The *a*, *b*, and *c* coefficients are determined using:

$$a_{H2} = 3.382 \times 10^{-6} \tag{12}$$

$$b_{H2} = 0.9727 \tag{13}$$

$$c_{H2} = 5.928e \times 10^{-6} \tag{14}$$

The rate of generated oxygen in the system is given as:

$$\dot{M}_{O2_{Out}} = a_{O2} \times \dot{W}_{PEM}^{\ b_{O2}} + c_{O2}\text{kg/s} \tag{15}$$

In equation (15), the value of a_{O2} is equal to 1.691×10^{-6}, the value of b_{O2} is equal to 0.9728, and the value of c_{O2} is equal to 2.978×10^{-6}.

3.3. Reverse osmosis (RO) desalination unit

Reverse osmosis is one of the new methods of purification and desalination of impure water. Reverse osmosis is a physical process that uses the phenomenon of osmosis, which means the difference in osmotic pressure between salt water and pure water, to remove salts and impurities from water. In this process, the raw water flow is divided into the product water flow and concentrated water flow.

This section examines the relations and conditions associated with the RO desalination unit analysis.

The power of the RO desalination unit pump was calculated as follows [94–96]:

$$\dot{W}_{RO\_Pump} = 0.15 \times \dot{W}_{\text{total}} = (1000 \times \Delta T_{\text{net}} \times M_{36})/(3600 \times \text{rho}_{36} \times \eta_{pump\_RO}) \tag{16}$$

where rho_{36} is the density of the input seawater, M_{36} is the molar mass of the input water, and $\eta_{pump,RO}$ is the efficiency of the RO desalination pump. The output power of the RO turbine is [94–96]:

$$\dot{W}_{RO\_Turbine} = (1000 \times \Delta T_{\text{net}} \times M_{39} \times \eta_{Turbine\_RO})/(3600 \times \text{rho}_{39}) \tag{17}$$

where $\eta_{pump,RO}$ is the efficiency of the RO desalination unit pump and ΔT_{net} is the temperature variation of the input water to the RO desalination unit. The net required power of the RO desalination unit was calculated as follows:

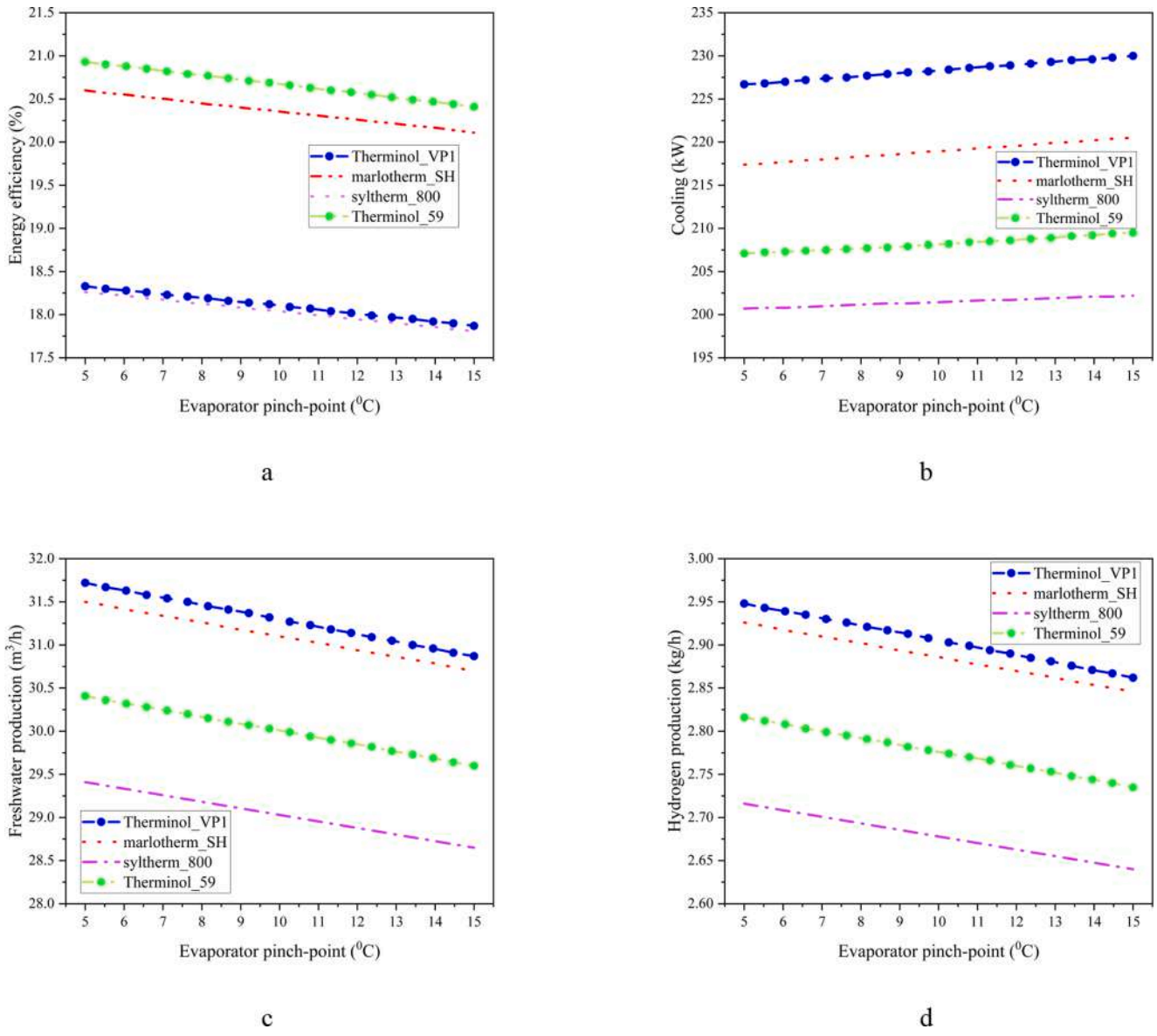

Fig. 7. Effect of the evaporator pinch-point temperature on system outputs (with different heat transfer fluids): **(a)** net output power, **(b)** cooling production, **(c)** freshwater production, **(d)** hydrogen production, € exergy efficiency, **(f)** energy efficiency, **(g)** cost rate, and **(h)** levelized cost.

$$\dot{W}_{net\_RO} = (\dot{W}_{RO\_Pump} - \dot{W}_{RO\_Turbine}) \tag{18}$$

3.4. Energy balance

The relations in Table 2 are used for the energy balance of the system components examined in the present study.

The total power of the SRC is given as:

$$\dot{W}_{net,\ steam} = \dot{W}_{turbine,\ steam} - \dot{W}_{pump1} \tag{19}$$

The total power of the ORC is calculated using:

$$\dot{W}_{net,\ ORC} = \dot{W}_{turbine,\ ORC} - \dot{W}_{pump2} - \dot{W}_{pump3} \tag{20}$$

Regarding the relations in Table 2, the net power output of the system performance is obtained using:

$$\dot{W}_{net} = \dot{W}_{net\_steam} + \dot{W}_{net,\ ORC} \tag{21}$$

3.5. Exergy analysis

The exergy of each flow is computed in this section. Table 3 displays the exergy destruction relation for each component.

The total exergy destruction rate of the absorber chiller is calculated using:

$$\dot{E}_{chiller} = \dot{E}_{G\_LiBr} + \dot{E}_{ABS\backslash\_LiBr} + \dot{E}_{C\_LiBr} + \dot{E}_{Eva\_LiBr} + \dot{E}_{p\_LiBr} + \dot{E}_{valve1\_LiBr} + \dot{E}_{valve2\_LiBr} + \dot{E}_{HEX\_LiBr} \tag{22}$$

The total exergy destruction rate of the electrolyzer is calculated using:

$$\dot{E}_{PEM} = \dot{E}_{32} + \dot{W}_{PEM} - \dot{E}_{33} - \dot{E}_{35} \tag{23}$$

The total exergy destruction rate of the RO desalination unit is calculated using:

$$\dot{E}_{RO} = \dot{E}_{37} + \dot{W}_{RO} - \dot{E}_{38} - \dot{E}_{39} \tag{24}$$

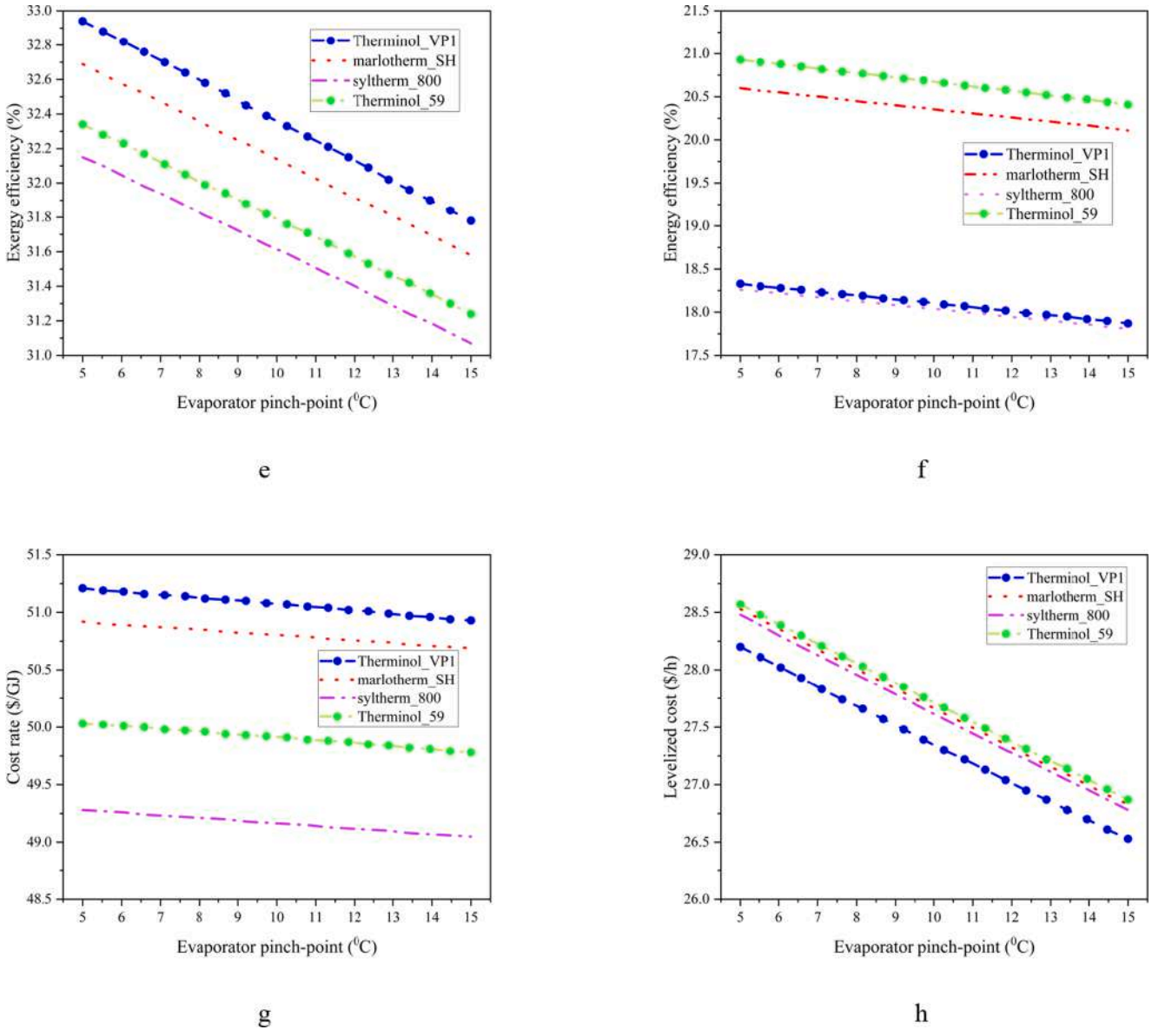

Fig. 7. (*continued*).

3.6. Economic analysis

The cost rate is obtained using economic parameters, such as the capital recovery factor (CRF) and interest rate, to achieve a thorough evaluation of the cost of the system. Because every component of a combined system is expected to operate at a specific time, the levelized cost rate of every component reflects a proper criterion for the cost rate symbolized by $\dot{Z}_k$. The levelized cost rate of every component is summed as the capital investment cost and operating and maintenance costs as [97–99]:

$$\dot{Z}_K = \dot{Z}_{K,CI} + \dot{Z}_{K,OM} \tag{25}$$

$$\dot{Z}_{K,CI} = \frac{CRF \cdot Z_K}{\beta} \tag{26}$$

$$\dot{Z}_{K,OM} = \frac{\phi \cdot Z_K}{\beta} \tag{27}$$

where Z_K is the purchase cost of the equipment (Table 4) and φ represents the maintenance and repair coefficients (herein, 1.06). Similarly, N is the number of operating hours of the system (7446). The CRF is given as [92,93]:

$$CRF = \frac{i(1+i)^n}{(1+i)^n - 1} \tag{28}$$

where i is the interest rate (which is equivalent to 0.1) and n denotes the plant operation period in years (20). Table 4 presents the relations linked to the cost of the components in addition to auxiliary relations.

3.7. Exergoeconomic analysis

A parameter, known as the flow cost rate ($\dot{C}$), is defined for every exergy flow of the system, and a cost-balance equation is written for every component. In addition, a (c) parameter is the defined cost per unit exergy. In an exergoeconomic analysis, the cost balance for every component of the system is expressed as [100–104]:

$$\dot{C}_{q,k} + \sum_i \dot{C}_{i,k} + \dot{Z}_k = \sum_e \dot{C}_{e,k} + \dot{C}_{w,k} \tag{29}$$

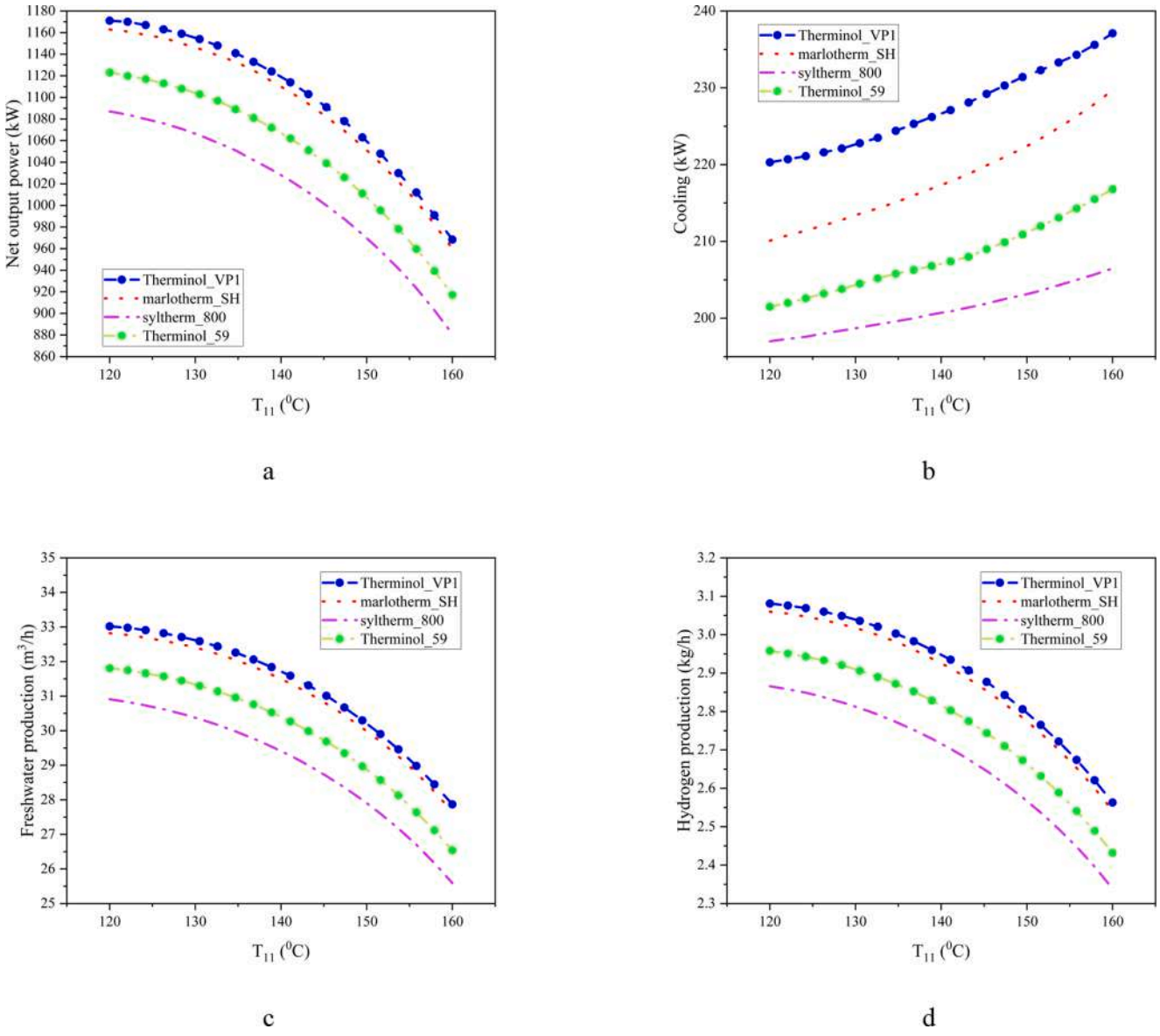

Fig. 8. Effect of the ORC turbine input temperature on system outputs (with different heat transfer fluids): **(a)** net output power, **(b)** cooling production, **(c)** freshwater production, **(d)** hydrogen production, **(e)** exergy efficiency, **(f)** energy efficiency, **(g)** cost rate, and **(h)** levelized cost.

$$\dot{C}_j = c_j \dot{E}x_j \tag{30}$$

Subscripts *e, w, q,* and *i* indicate the output, work, heat, and input exergy cost, respectively. The final costs of the components of the system are listed in Table 5.

3.8. Integrated system

By integrating the poly-generation system, the following equations were used to estimate the energy and exergy efficiencies of the system:

$$\eta_{en} = (\dot{W}_{net\_steam} + \dot{W}_{net\_ORC} + \dot{Q}_{cooling} + (\mathrm{hhv}_{h2} \times \dot{m}_{33}) - \dot{W}_{net\_PEM} - \dot{W}_{net,RO})/\left(\dot{Q}_{u2} + \dot{m}_1 \times h_1\right) \tag{31}$$

$$\eta_{ex} = (\dot{W}_{net\_steam} + \dot{W}_{net\_ORC} + \dot{E}x_{cooling} + \dot{E}x_{38} + \dot{E}x_{32} + \dot{E}x_{33} + \dot{E}x_{35} - \dot{W}_{net\_PEM} - \dot{W}_{net\_RO})/(\dot{E}x_1 + \dot{E}x_{sun}) \tag{32}$$

4. Validation

To validate the research, two energy-producing units from this system were selected for validation. Because the poly-generation energy system proposed in this study is novel, the RO desalination unit subsystem is compared with that of Nafey et al. [105] (Table 6). As the results of this validation show, the results obtained for the modeling of the reverse osmosis desalination unit of the present work have a low error compared to the reference research and indicate the accuracy of the modeling.

To increase the credibility of the research, the hydrogen production unit was also selected for validation. The PEM electrolyzer results are compared with the data of Ioroi et al. [106] (Fig. 2) to validate the results. The modeling procedure and results were validated based on the results.

The specifications of the electrolyzer used in the system have been checked. The information required for electrolysis is introduced in Table 7.

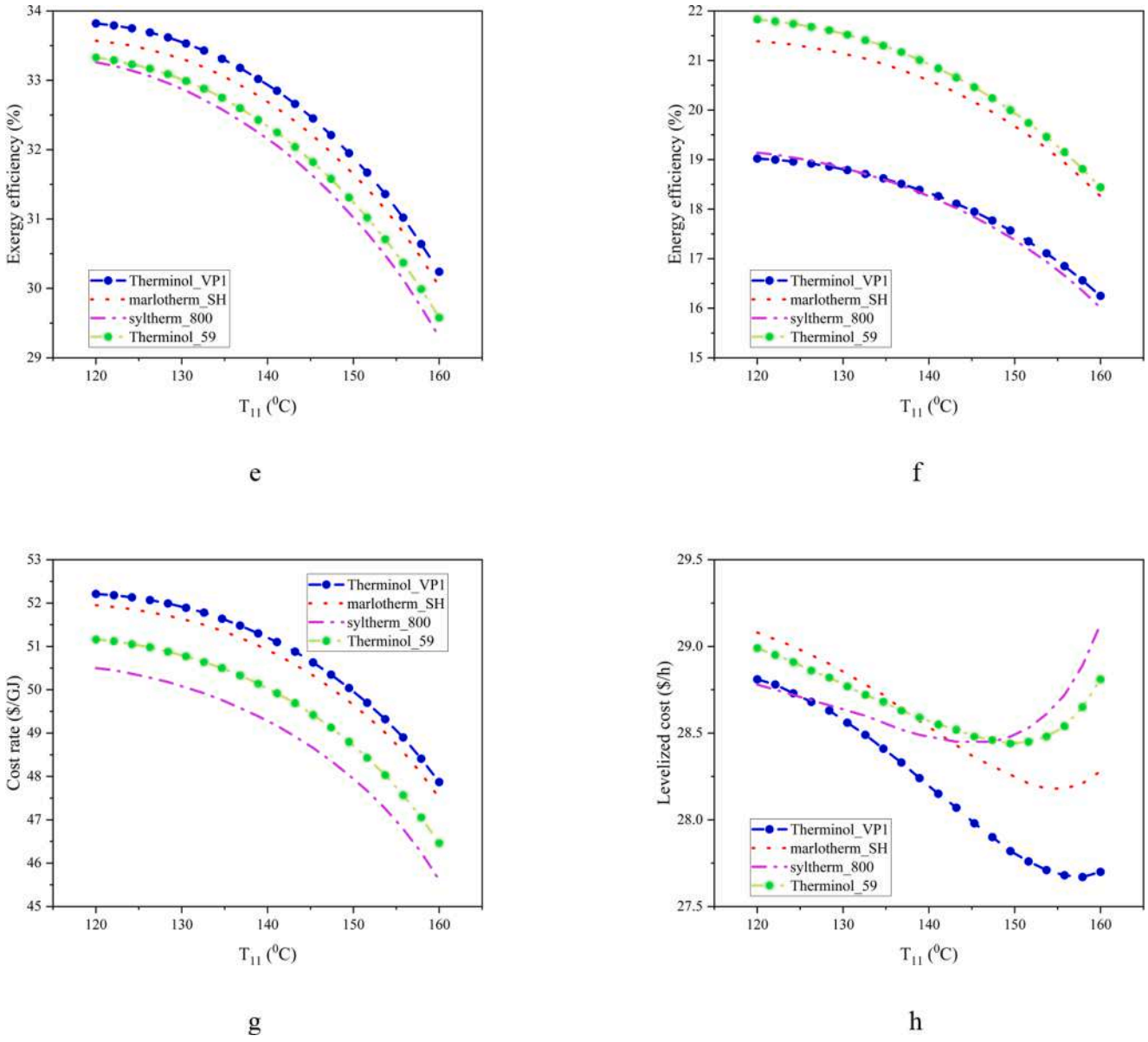

Fig. 8. (*continued*).

5. Results and discussion

5.1. Parametric analysis

Discovering the optimal solution for the system efficiency and its costs and determining the system-impacting parameters are the main challenges in analyzing energy-generating systems that employ renewable energy. Herein, the parameters (i.e., net output power, cooling, hydrogen, and freshwater, as well as exergy and energy efficiencies, cost rate, and levelized cost) are analyzed to determine the effects of heat transfer fluids on system outputs. Different parameters were analyzed, including the SRC turbine outlet pressure, ORC condenser temperature, SRC turbine input pressure, pump efficiency, input temperature to the ORC turbine, and input pressure to the open feedwater heater. In addition, the solar radiation intensity, geothermal fluid mass flow rate, turbine efficiency, and evaporator pinch-point temperature substantially affected the system performance; only the results of these four parameters are delineated in the following.

Table 8 lists the properties of the four heat transfer fluids selected for employment in the parabolic solar collector, and they are used in the modeling and simulation of the system.

5.1.1. Solar radiation intensity

First, the effect of solar radiation intensity variations in the 450–950 W/m^2 range on the system outputs and parameters for different heat transfer fluids is investigated (Fig. 3). Solar radiation intensity is among the most fundamental parameters affecting the thermal efficiency of solar systems. Solar radiation intensity increases and decreases as the sun rises and sets, respectively; however, its rate of change is maximal when the distance between the sun and earth varies. Solar radiation determines the rate of the output efficiency of a solar system. The efficiency and performance of solar collectors are highly dependent on solar radiation intensity because the entire energy required by solar collectors for energy generation is supplied by sunlight. As the solar radiation intensity increased, the net output power of the system increased, and the best result was associated with the Therminol 59 heat transfer fluid

Table 9
Sensitivity analysis.

Row	Objective Function Parameter	Exergy Efficiency (%)	Energy Efficiency (%)	Levelized Cost ($/Gj)	Cost Rate ($/h)
1	**ORC turbine input temperature (^{0}C)**	Max: 33.82 Min: 30.24 −11.83%	Max: 19.02 Min: 16.25 −17.04%	Max: 28.81 Min: 27.7 −4.01%	Max: 52.21 Min: 47.87 −9.06%
2	**Pump efficiency (%)**	Max: 32.95 Min: 32.88 +0.21%	Max: 18.34 Min: 18.29 +0.27%	Max: 28.29 Min: 28.17 −0.42%	Max: 51.24 Min: 51.2 −0.08%
3	**Turbine efficiency (%)**	Max: 36.42 Min: 31.77 +14.63%	Max: 21.29 Min: 17.33 +22.85%	Max: 31.15 Min: 27.16 +14.69%	Max: 54.31 Min: 50.14 +9.11%
4	**Solar collector mass flow rate (kg/h)**	Max: 35.24 Min: 30.39 +15.95%	Max: 18.91 Min: 17.93 −5.46%	Max: 32.22 Min: 28.28 −13.93%	Max: 54.71 Min: 46.96 +16.51%
5	**Solar radiation intensity (W/m^2)**	Max: 38.88 Min: 32.12 −21.04%	Max: 18.46 Min: 17.65 +4.58%	Max: 30.02 Min: 28.5 +5.33%	Max: 52.03 Min: 47.23 +10.16%
6	**Evaporator pinch-point temperature (^{0}C)**	Max: 32.94 Min: 31.78 −3.65%	Max: 18.33 Min: 17.87 −2.43%	Max: 51.21 Min: 50.93 −0.55%	Max: 28.2 Min: 26.53 −6.29%

(increased from 800 to 1200 kW). This is because, as the solar intensity increases, the heat transfer from the collector to the heat transfer fluid and thereof to the geothermal fluid increases, which elicits a higher output power (a). The system-produced cooling is enhanced, and the best result of cooling production is related to Therminol 59 (b). The rates of freshwater and hydrogen generated by the system increased when the solar radiation intensity increased, and the best production result was obtained with Therminol 59 (c and d) The exergy efficiency of the system decreased, and the best exergy result was related to Therminol 59 (e) Further, the energy efficiency increases, but the best result for energy efficiency is associated with Therminol VP1 (f). The cost rate of the system increments as the solar radiation intensity increases, and the results show that the lowest and highest cost rates are linked to Syltherm 800 and Therminol 59, respectively (g) (Fig. 3 a-g). The levelized cost rate of the system increased, and the results revealed that the minimum and maximum cost rates were associated with Syltherm 800 and Therminol 59, respectively (h). The rising cost rate of the system can be attributed to the fact that they are directly interrelated; that is, the need for larger and energy-consuming equipment and installations increases with the increase in the total power of the system, augmenting the system cost. Therefore, solar radiation can be one of the most effective parameters in the proposed system.

5.1.2. Solar collector mass flow rate

The effect of the solar collector mass flow rate, ranging from 10 to 20 kg/h, on the system outputs and parameters for different heat transfer fluids is investigated (Fig. 4). An upsurge in the mass flow rate of the solar collector increases the total power of the system. Fig. 4**a** shows that the rate of power of the system increases with an increase in the mass

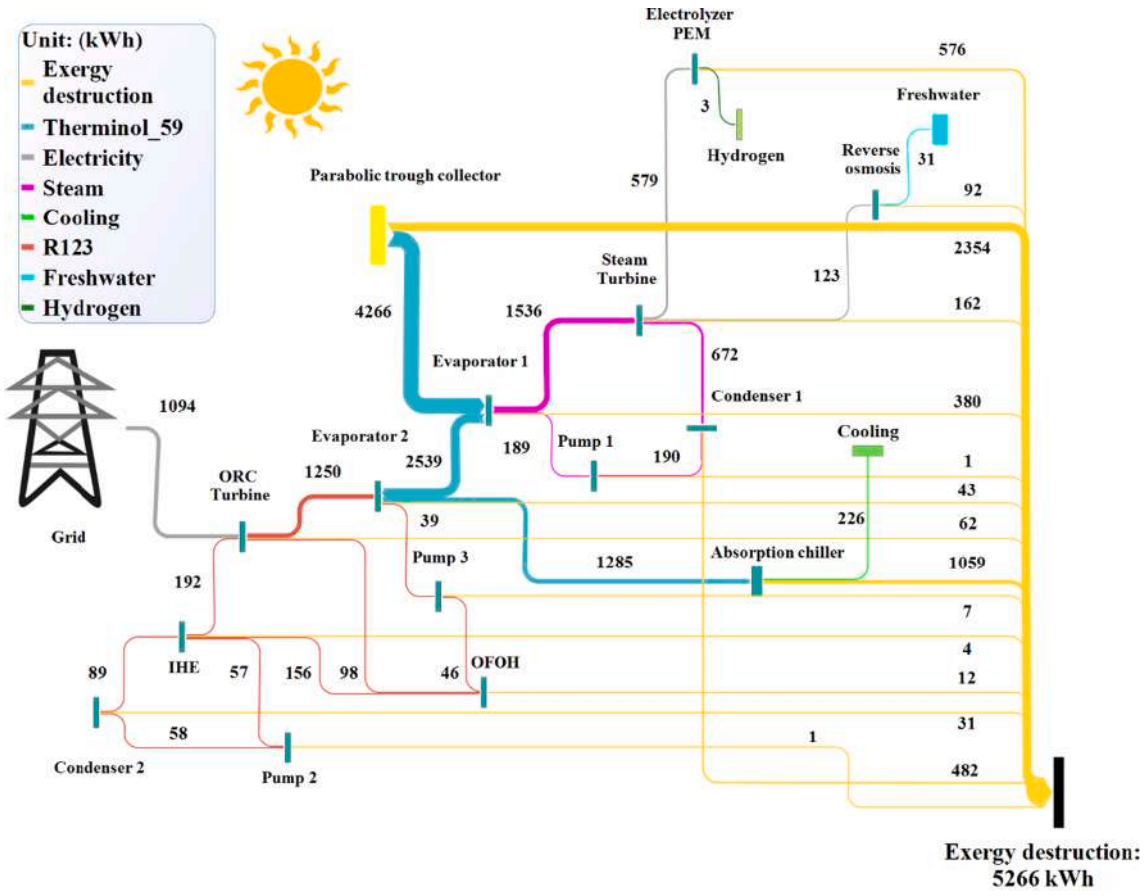

a

Fig. 9. Grossman diagram for system exergy analysis. of **(a)** Therminol 59, **(b)** Marlotherm SH, **(c)** Syltherm 800, and **(d)** Therminol VP1.

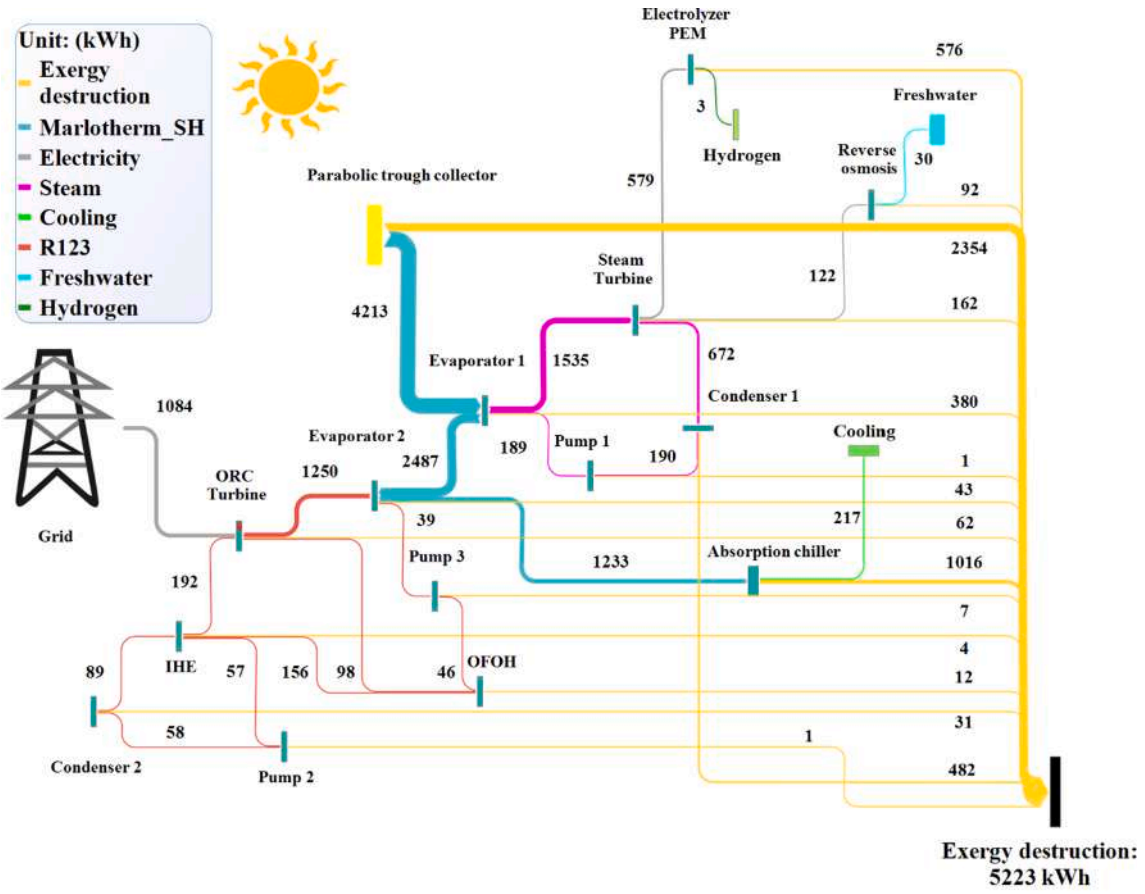

b

Fig. 9. (*continued*).

flow rate of the solar collector, and the best result of the net output power is related to the Therminol 59 heat transfer fluid. Fig. 4**b** illustrates that the cooling production of the system increases as the mass flow rate of the system increases, and the best result for cooling production is connected to the Therminol 59 heat transfer fluid. Fig. 4**c** and Fig. 4**d** show that the rates of the generated freshwater and hydrogen increased when the mass flow rate of the solar collector increased, and the best production result was associated with the Therminol 59 heat transfer fluid. As shown in Fig. 4**e**, the exergy efficiency of the system increased as the mass flow rate of the solar collector increased. Therefore, the exergy efficiency and power of the system are directly interrelated, and the best result is related to Therminol 59.

Fig. 4**f** displays that the system energy declined, and the best energy-efficiency result was linked to Therminol VP1. The cost rate of the system is amplified, and the results show that the minimum and maximum cost rates are related to the heat transfer fluids of Syltherm 800 and Therminol 59, respectively (Fig. 4**g**). The levelized cost of the system increases as the mass flow rate of the solar collector increases (Fig. 4**h**). The results reveal that the lowest and highest costs are linked to the heat transfer fluids of Therminol 59 and Therminol VP1, respectively.

5.1.3. Turbine efficiency

This section investigates the effect of turbine efficiency in the 0.75–0.95 range on system outputs and the parameters for different heat transfer fluids (Fig. 5). Turbine efficiency is the ratio of the output power to the total input power. Fig. 5**a** shows that the power of the system is enhanced when the turbine efficiency improves. Further, the best and weakest results for the net output power are related to the heat transfer fluids of Therminol 59 and Syltherm 800, respectively. The produced cooling of the system does not change, although the turbine efficiency increases and its value remains constant (Fig. 5**b**). However, the best cooling production result was related to the Therminol 59 heat transfer fluid. Fig. 5**c** and Fig. 5**d** depict that the rates of freshwater and hydrogen escalated, and the best results were related to Therminol 59.

Fig. 5**e** and Fig. 5**f** demonstrate that the exergy and energy efficiencies of the system are directly enhanced by the turbine efficiency. This is because the exergy efficiency and output power of the system are directly interrelated. The results revealed that the best exergy and energy efficiencies were related to Therminol 59. Fig. 5**g** depicts that the cost rate of the system increased. The results revealed that the minimum and maximum cost rates were related to Syltherm 800 and Therminol 59, respectively. The level of the system increased with an increase in turbine efficiency (Fig. 5**h**). The results indicate that the minimum and maximum costs were associated with Therminol 59 and Therminol VP1, respectively.

5.1.4. Pump efficiency

This section investigates the effect of pump efficiency in the 0.75–0.95 range on the system outputs and the parameters for different heat transfer fluids (Fig. 6). The pump efficiency is defined as the ratio of the fluid-obtained operative power to the total power. In mathematical terms, pump efficiency is the ratio of the pressure to its enthalpy. The net output power, cooling, freshwater, and hydrogen production; exergy and energy efficiency; and cost rate increase gradually with the Therminol 59 heat transfer fluid performing better than the others (Fig. 6**a–6 g**). However, regarding levelized cost, all heat transfer fluids follow a declining trend, and the Therminol 59 heat transfer fluid encompasses the least levelized cost. Regarding energy efficiency, the Therminol VP1

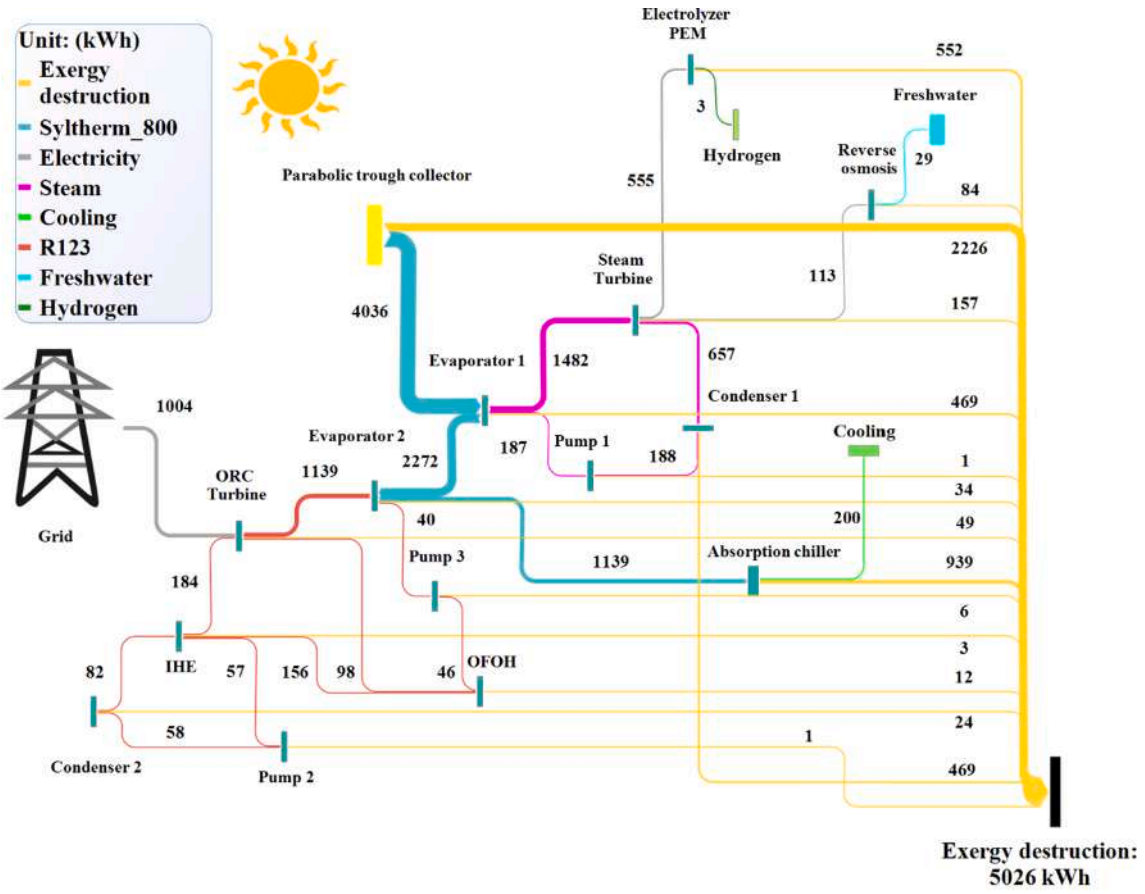

C

Fig. 9. (*continued*).

leads compared with other heat transfer fluids. In all system outputs, Syltherm 800 had the lowest performance.

5.1.5. *Evaporator pinch-point temperature*

This section examines the effect of the evaporator pinch-point temperature in the 5–15 °C range on the system outputs and parameters for different heat transfer fluids (Fig. 7). The pinch-point temperature is an important parameter that affects heat transfer to the SRC. The output power of the system increases with an uptrend in the pinch point temperature (Fig. 7**a**). Further, the strongest and weakest output powers are related to the heat transfer fluids of Therminol 59 (from 1117 to 1086 kW) and Syltherm 800 (from 1027 to 998.5 kW) in the PTSC, respectively. With the increase in the pinch-point temperature, the rate of heat transfer to the SRC declines, reducing the net output power of the system. Therefore, the increase or decrease in the heat transfer rate was directly related to the output power of the system. Fig. 7**b** shows that, due to an increase in the evaporator pinch-point temperature, the produced cooling of the system increases, and the best cooling production result is connected to Therminol 59.

The rates of the generated freshwater and hydrogen decrease, and the best result is related to the Therminol 59 heat transfer fluid (Fig. 7**c** and Fig. 7**d**). An increase in the pinch-point temperature of the evaporator causes a decline in exergy (from 33.88% to 32.78%) and energy efficiencies of the system due to the direct relationship with the net output power of the system (Fig. 7**e** and Fig. 7**f**). The results reveal that the best exergy and energy efficiencies are related to the Therminol 59 heat transfer fluid. The cost rate of the system is reduced (Fig. 7**g**). The figure shows that the minimum and maximum cost rates are connected to the heat transfer fluids of Syltherm 800 and Therminol 59, respectively. Fig. 7**h** illustrates that the levelized cost of the system decreased as the evaporator pinch-point temperature increased. Therefore, the minimum and maximum costs are related to the heat transfer fluids of Therminol 59 (from 28.11 to 26.53 $/h) and Therminol VP1 (from 28.57 to 26.87 $/h), respectively.

5.1.6. *ORC turbine input temperature*

This section examines the effect of the evaporator pinch-point temperature in the 120–160 °C range on the system outputs and parameters for different heat transfer fluids (Fig. 8).

The net output power of the system declines when the ORC turbine inlet temperature increases and the best result for the output work are related to the Therminol 59 heat transfer fluid (Fig. 8**a**). The maximum net output power at 120 °C can be expressed as follows. According to the energy balance of the ORC evaporator, and with an increase in the ORC turbine input temperature, the enthalpy of stream 11 increased, and the mass flow rate of the ORC decreased. This leads to a reduction in the net output power. Fig. 8**b** displays that the cooling production increments at a low gradient escalated, and the best production result was obtained with the Therminol-59 heat transfer fluid. Freshwater and hydrogen production followed a similar decreasing trend (Fig. 8**b** and Fig. 8**c**) as the ORC turbine input temperature increased. The best performance in both cases was also associated with the Therminol 59 heat transfer fluid. The exergy and energy efficiencies of the system decrease because the exergy efficiency and net output power of the system are directly interrelated (Fig. 8**d** and Fig. 8**f**,). The best results for the exergy and energy efficiencies are associated with the Therminol 59 heat transfer fluid.

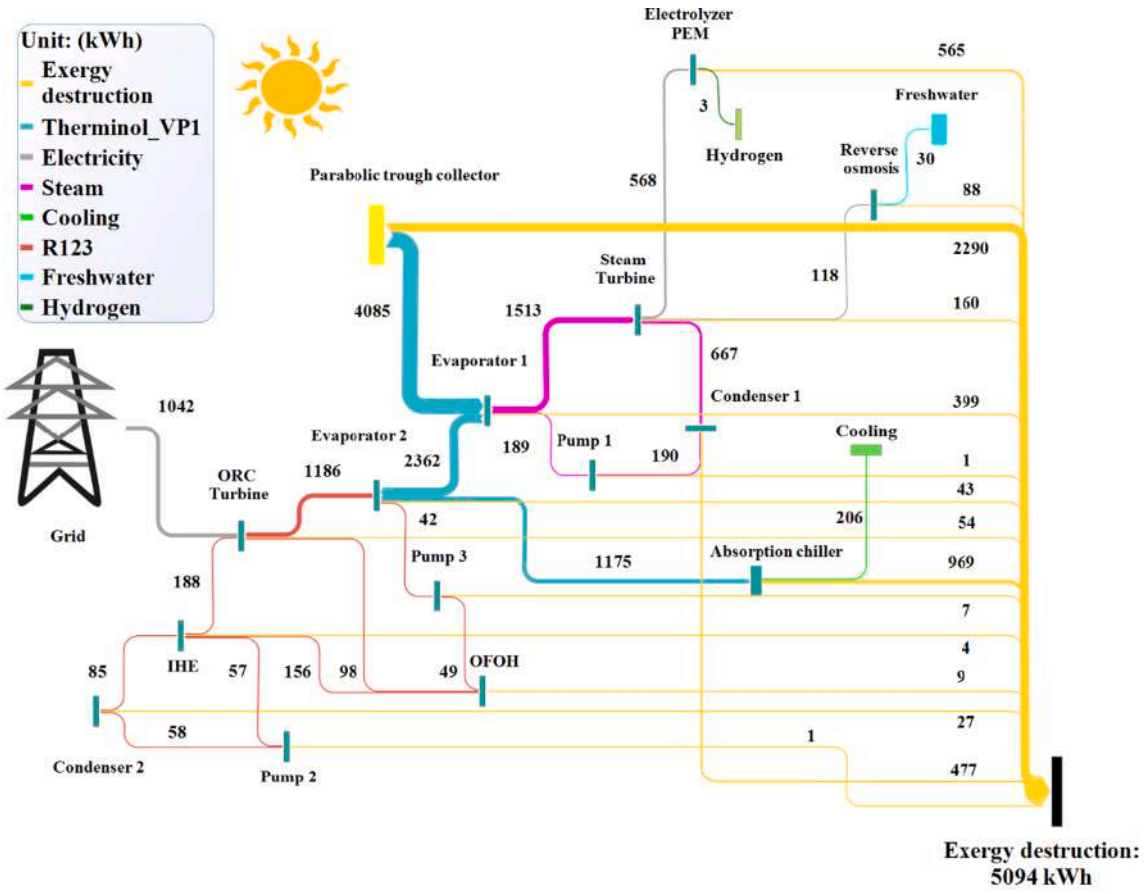

d

Fig. 9. (*continued*).

Table 10
Energy analysis and exergy destruction.

Collector oil	Exergy destruction (kWh)	Power (kWh)	Cooling (kWh)	Hydrogen (kg/h)	Freshwater (m^3/h)
Therminol 59	5266	1094	226	3	31
Marlotherm SH	5223	1084	217	3	30
Syltherm 800	5026	1004	200	3	29
Therminol VP1	5094	1042	206	3	30

The cost rate of the system also decreases as the ORC turbine input temperature increases (Fig. 8**g**) because a decline in the system output leads to a decrease in the cost rate. The results reveal that the minimum and maximum cost rates are associated with the heat transfer fluids of Syltherm 800 and Therminol 59, respectively. The levelized cost of the system decreases when the ORC turbine input temperature increases to approximately 150 °C (Fig. 8**h**); thereafter, the levelized cost begins to increase. The results reveal that the minimum and maximum levelized costs are related to the heat transfer fluids of Therminol 59 and Therminol VP1 on average, respectively.

The main challenge in the analysis of energy production systems that are designed based on the use of renewable energy is to find the most optimal and best solution for the efficiency of the system, its costs and determining the parameters affecting the system.

External costs are the harmful results of economic activities and these costs appear as destructive effects on the environment. Energy production from power plants and facilities causes the environment to incur costs that are not included in the final price of that product. Failure to pay attention to the environmental costs of electricity production causes destructive effects on natural resources, in the country's energy system, external costs imposed on the environment cause air pollution, reduction of freshwater resources, etc. By substituting new and renewable energies, we can help reduce these costs.

5.2. Sensitivity analysis

Using sensitivity analysis is one of the effective methods for simplifying numerical models. In the models that are built to simulate the behavior of multiple energy production cycles, there are a large number of variables that do not necessarily all have the same effect on the output of the model. Therefore, using sensitivity analysis methods, less important variables can be identified and kept constant in their nominal values, and modeling and predictions can be made based on more sensitive variables to save time and money. In this study, the analysis of the sensitivity of the design parameters on the performance of the system has been investigated. The results of sensitivity analysis on the main output of the system, including exergy efficiency, energy efficiency, levelized cost, and cost rate for Therminol 59 oil as the best lubrication for the parabolic collector, are reviewed in Table 9. This analysis is calculated to investigate the effect of changes in design parameters on the technical and economic performance of the system.

It should be noted that in this table, the positive sign (+) indicates the percentage growth of the objective function and the negative sign (-) indicates the percentage decrease of the objective function. To show the effect of six design parameters and the effect of each parameter on the

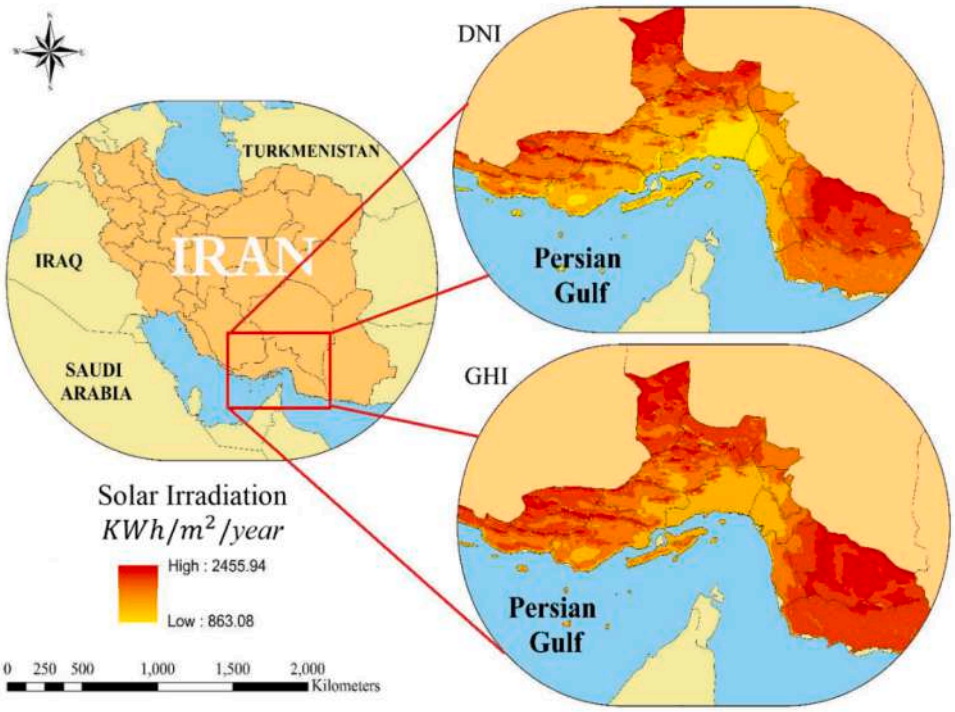

a

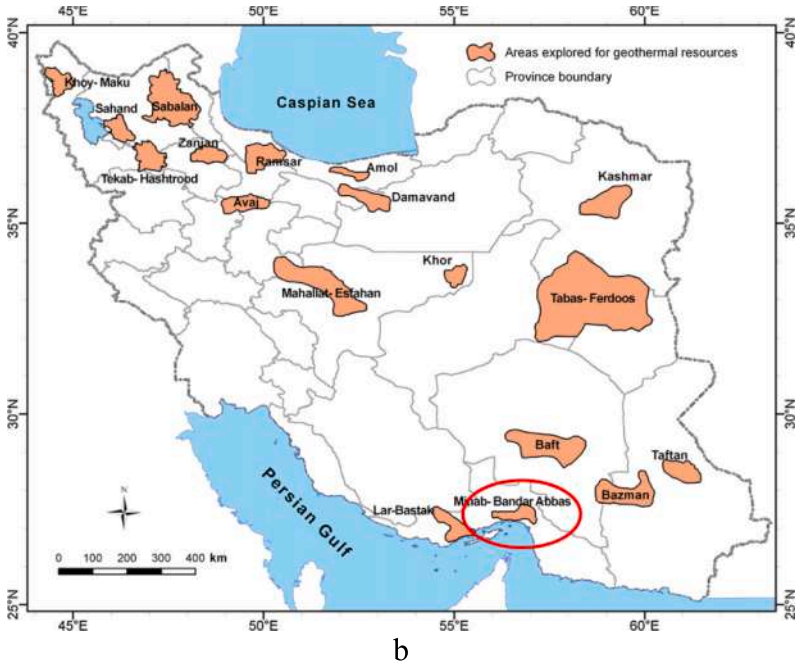

b

Fig. 10. Location of Bandar Abbas on Iran's map regarding **(a)** annual direct normal irradiance (DNI) and global horizontal irradiance (GHI) [107] and **(b)** Iran's geothermal resources map [108].

technical and economic performance of the system, the effect of these parameters has been calculated in Table 9. The results show that the increase of two parameters, Evaporator pinch-point temperature, and ORC turbine input temperature, reduces the technical performance of the system, and due to the reduction of the system performance and the reduction of the hidden and visible costs of the system due to the maintenance of the system, it also decreased. But the increase of two parameters of turbine efficiency and intensity of solar radiation increases the performance of the system, and due to the increase in production and the need for maintenance, the costs of the system also increase. As the results show, Turbine efficiency, Solar radiation intensity, Solar collector mass flow rate, and ORC turbine input temperature parameters had the greatest effect on the objective functions. It has had the least impact on the target functions, respectively, the Pump efficiency and Evaporator pinch-point temperature parameters.

In the following, the effect of the parameters on the objective functions is briefly discussed:

- The reason for the increase in the cost and cost rate of the system in the studies carried out can be related to the fact that the cost and the

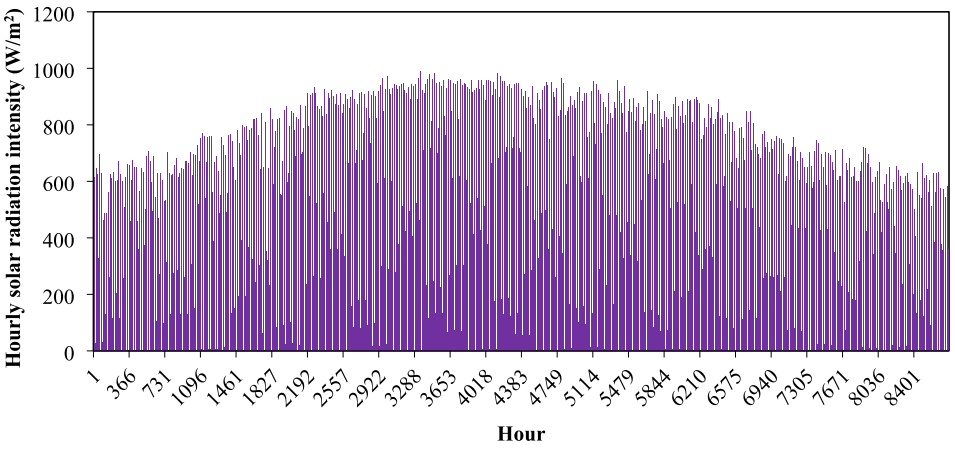

Fig. 11. Hourly solar radiation intensity variations in Bandar Abbas during the year (MeteoNorm Software) [109].

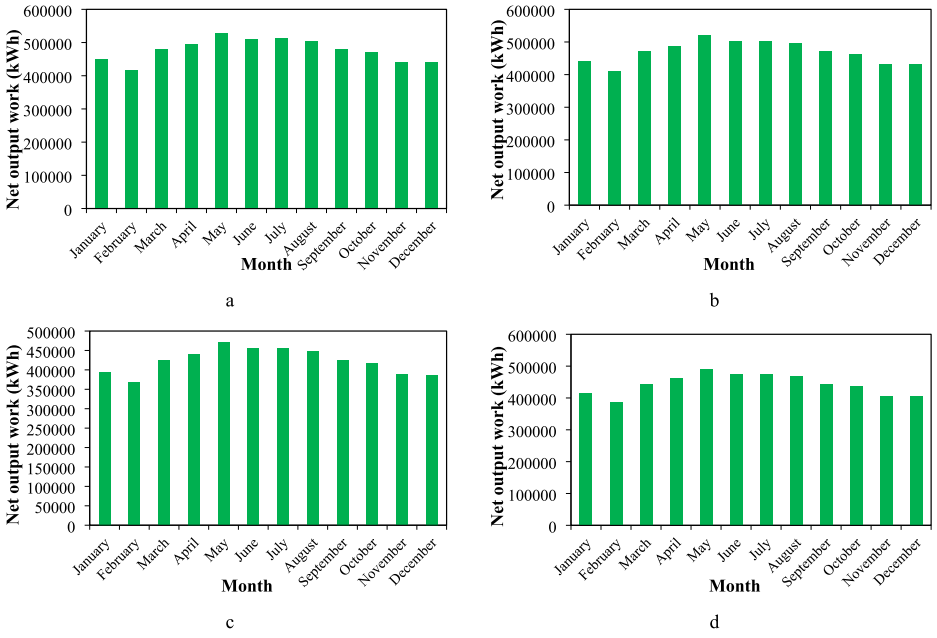

Fig. 12. Results of solar radiation intensity variations during the year on the net output work of the system with the heat transfer fluids of **(a)** Therminol 59, **(b)** Marlotherm SH, **(c)** Syltherm 800, and **(d)** Therminol VP1.

work output of the system have a direct relationship, that is, as the total work increases, the need for larger and more consuming equipment and facilities increases and As a result, it increases the cost of the system.

- The costs of finding and hiding the failure of equipment, devices, and subsystems are significant. If the maintenance and repair costs of the devices are discussed, mainly the obvious costs have been examined, also the obvious costs can be mentioned the cost of manpower and repairs. It should be said that the hidden costs of the system also affect the overall costs of the system, which can be attributed to the costs of non-production during machine downtime, and the costs of providing low-quality spare parts that lead to repeated failures. Be and … pointed out.
- The intensity of the sun's radiation increases or decreases with the sunrise and sunset, but its main changes are greater when the distance of the earth from the sun changes. Solar radiation determines the output power performance of a solar system. The performance and efficiency of solar collectors depend more on the intensity of solar radiation than any other factor, because all the power required to produce energy is provided by solar collectors from sunlight, and the higher the amount of solar radiation, the more efficient the solar collectors will be. Found.
- The intensity of solar radiation on the absorbing plate of this energy in renewable systems is a factor that has a significant impact on the performance of solar systems.
- As the intensity of solar radiation increases, the flow rate of the input fluid to the solar system increases, and as a result, with the increase of the input flow rate to the collector, the output work of the turbine increases, which will increase the total output work, and vice versa.
- With the increase in the intensity of solar radiation, the flow rate of the input fluid to the parabolic-linear solar collector is increased, and as a result of the increase of the input flow rate to the collector, there will be a direct effect on the increase of the total output work, and vice versa.
- Pump efficiency is generally the ratio of the practical power obtained by the fluid to the total power, and in mathematical terms, pump efficiency is the pressure ratio to the pump enthalpy ratio.
- Turbine efficiency means the ratio of practical power to total power.
- As the pinch point of the evaporator increases, the amount of heat transfer decreases. By reducing the heat transfer from the evaporator

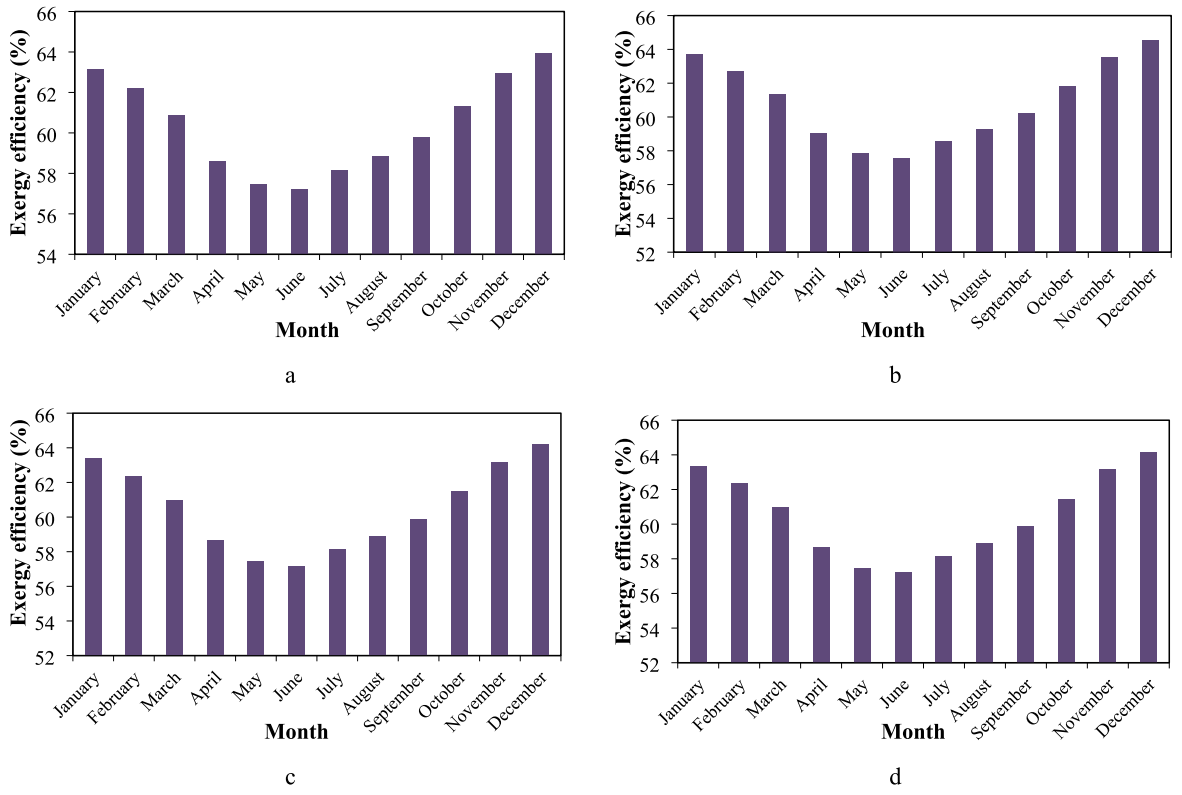

Fig. 13. Effect of variations in solar radiation intensity during the year on the exergy efficiency of the system with the heat transfer fluids of **(a)** Therminol 59, **(b)** Marlotherm SH, **(c)** Syltherm 800, and **(d)** Therminol VP1.

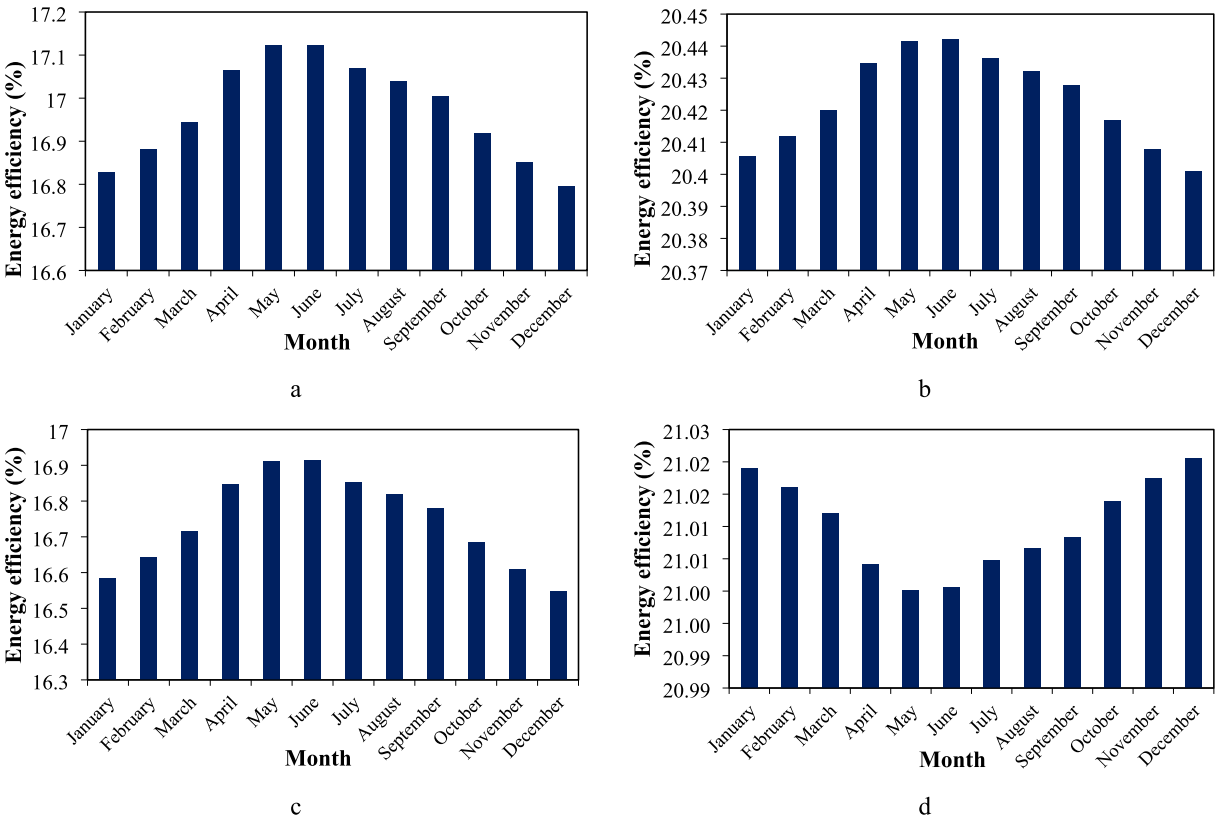

Fig. 14. Effect of variations in the solar radiation intensity during the year on the energy efficiency of the system with the heat transfer fluid of **(a)** Therminol 59, **(b)** Marlotherm SH, **(c)** Syltherm 800, and **(d)** Therminol VP1.

Table 11
System outputs during a year according to solar radiation variations in Bandar Abbas.

Heat transfer fluid	Output					
	Average energy efficiency (%)	Average exergy efficiency (%)	Net output work (kWh)	Cooling Production (kWh)	Freshwater production (m^3)	Hydrogen production (kg)
Therminol 59	16.97	60.37	5741637.46	1935793.92	169802.66	15370.99
Marlotherm SH	20.42	60.84	5618605.54	1844962.47	166365.84	15051.24
Syltherm 800	16.74	60.48	5070647.99	1729592.25	151184.3064	13628.74
Therminol VP1	21.01	60.47	5308404.50	1765713.00	157783.60	14245.74

Table 12
Number of households supported by the system.

Heat transfer fluid	Net output work (kWh)	Number of households
Therminol 59	5741637.46	196
Marlotherm SH	5618605.54	192
Syltherm 800	5070647.99	173
Therminol VP1	5308404.50	181

to the steam Rankine cycle, the work output of the entire system is also reduced. So it is concluded that increasing or decreasing the amount of heat transfer affects the work of the whole system and the efficiency of the system.

5.3. Sankey analysis

Exergy destruction means the rate of exergy loss in the system. The exergy destruction ratio shows the overall efficiency of the system. In general, exergy is the maximum useful work of a system, and destruction of exergy means the destruction of useful work or disruption of the process of useful output work. Analyzing exergy in renewable systems based on the first and second laws of thermodynamics makes it possible to identify the optimal method of analyzing energy systems and unfavorable thermodynamic processes affecting a system.

Exergy analysis consists of two steps, the first step is to identify and investigate undesirable thermodynamic processes of the system based on the determination of exergy waste. Exergy destruction is obtained by writing the exergy balance in different parts of the system and for the system components. The second step is to determine the most possible corrections in the system based on the concepts of avoidable exergy destruction. The minimum amount of exergy in the system during a process that cannot be prevented with existing techniques and economic considerations is called unavoidable exergy waste.

Exergy analysis is a fundamental step towards understanding and improving the quality of system performance by finding the main sources of exergy degradation. Fig. 9 shows the Grossman diagram in optimal conditions, which is a powerful tool for exergy analysis and graphically shows the exergy rate of each stream and the exergy destruction of all components.

For a correct understanding of the 4 examined oils, their exergy diagrams have been drawn. In this system, steam and organic Rankine cycle pumps had the lowest acrogen losses. The exergy analysis of the system showed that the highest exergy destruction is related to PTC, absorption chiller, ORC unit, SRC unit, PEM electrolyzer, and reverse osmosis respectively. To start the process, a solar input exergy rate is entered into the solar collector which The system provides for the start of the activity. The highest production power of the system is related to Therminol_59, marlotherm_SH, Therminol_VP1, and syltherm_800 oil respectively. Also, exergy analysis showed that the highest amount of

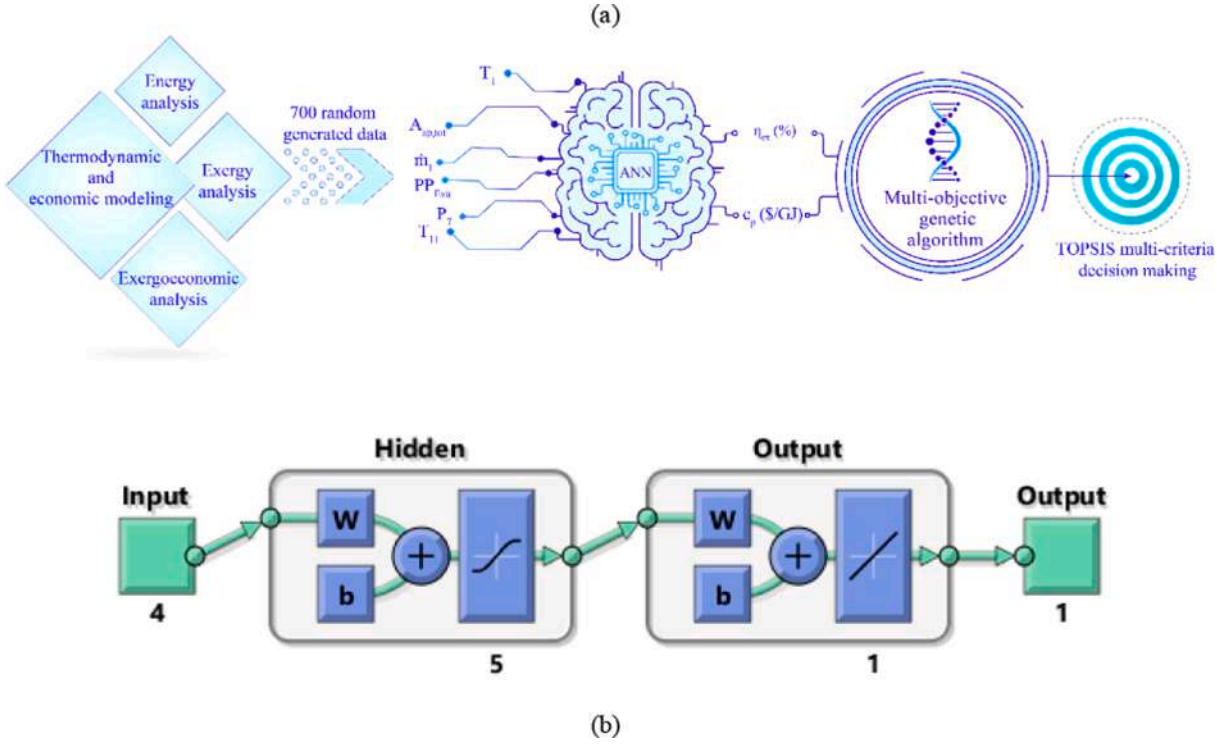

Fig. 15. (a) Flowchart of the optimization methodology. (b) Architecture of the neural networks.

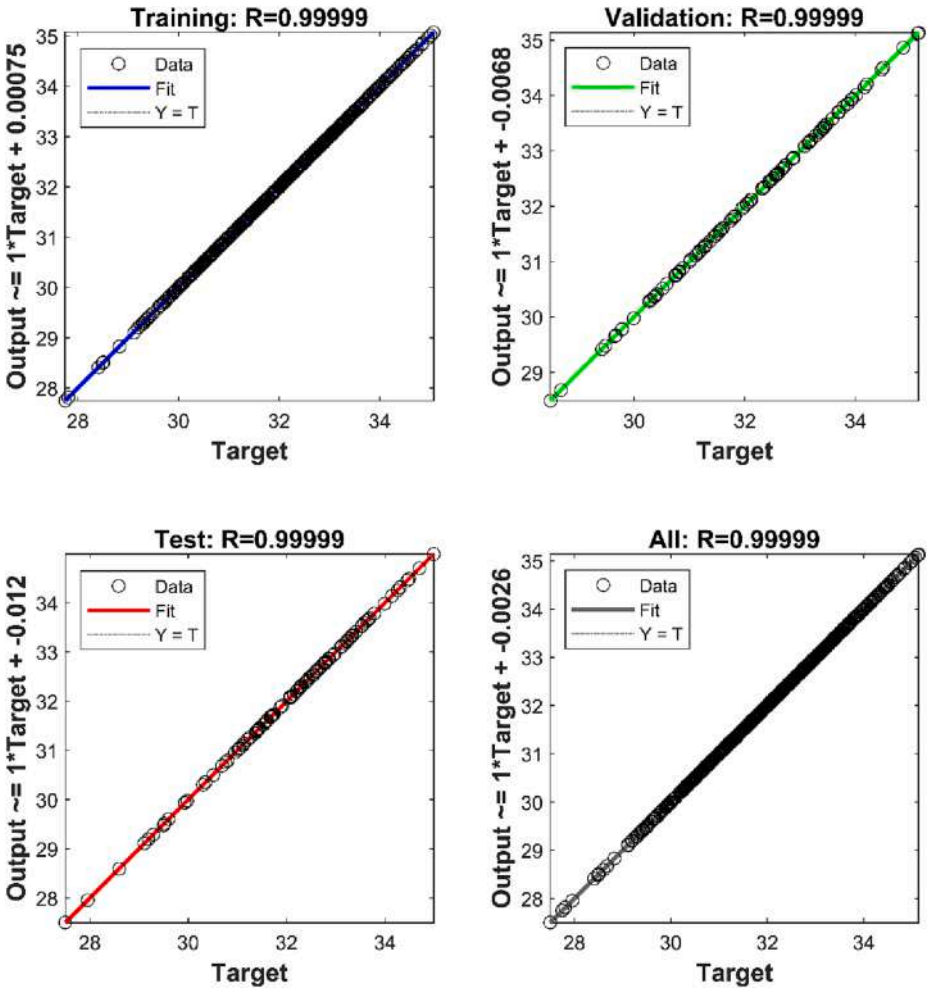

Fig. 16. Validation of the ANN algorithm for the objective function (Exergy Efficiency).

exergy destruction is when using Therminol_59, marlotherm_SH, Therminol_VP1, and syltherm_800 oil, respectively.

One of the reasons for exergy destruction in the solar collector is the fluid heating process, and because the evaporation process is irreversible the amount of irreversibility in it is greater than in other processes, it is obvious that in order to optimize the solar system, It focused on system components that perform irreversible processes.

One of the reasons for low exergy destruction in the pump is that the pump is only responsible for pumping the fluid and no irreversible process is performed in it. Also, the amount of irreversibility in it is very low compared to other processes, so exergy destruction is very low in it.

In Table 10, the amount of energy and exergy destruction of the investigated system components has been investigated, and for this reason, the amount of exergy destruction of the entire system, production power, production cooling, production hydrogen, and production freshwater of the system in four different modes of using oil for the parabolic collector It is calculated.

As the results showed, the best production power and performance of the system has been calculated when using Therminol 59 oil, and due to the increase in high performance of the system and the absorption of more thermal energy, the amount of exergy destruction also increased when using Therminol 59 oil.

5.4. Case study: Bandar Abbas

Bandar Abbas is Iran's largest port and the capital of Hormozgan Province. It is located in the south of the province and is bordered to the north by mountains and to the south by the Persian Gulf. In this city, almost three seasons of the year are summer, with vernal and desirable climates for solar systems. Fig. 10 illustrates the location of Bandar Abbas on Iran's map regarding very high solar irradiation and suitable geothermal potential.

Because of the proper location of Bandar Abbas in terms of its solar radiation potential and geothermal energy, this city was selected as a case study for the present research. The hourly solar radiation intensity variations during the year in Bandar Abbas are depicted in Fig. 11. Therefore, the MeteoNorm software [80] was used for acquiring the data related to this city.

There is a direct relationship between solar radiation and ambient temperature. As the intensity of solar radiation increases, thermal energy also increases, and for this reason, the temperature of the environment is the highest on the days when solar radiation increases. As the results show, there is the highest rate of solar radiation in June, July and August in the summer season. The changes in solar radiation in Bandar Abbas during the year are between 0 and 1000 W/m^2.

Solar systems operate based on the generation of clean electricity by absorbing radiated solar energy. Solar collectors are the most important equipment in power-generating systems and supply the requisite energy for the generation of clean energy by absorbing solar energy via their absorber plates. The results of the current survey reveal that the system's net output work, as well as freshwater and hydrogen production, are maximal in May and July (spring and summer), whereby solar radiation intensifies, enhancing the thermal energy of the system. Similarly, to the increase in the output work, the system costs will subsequently increase

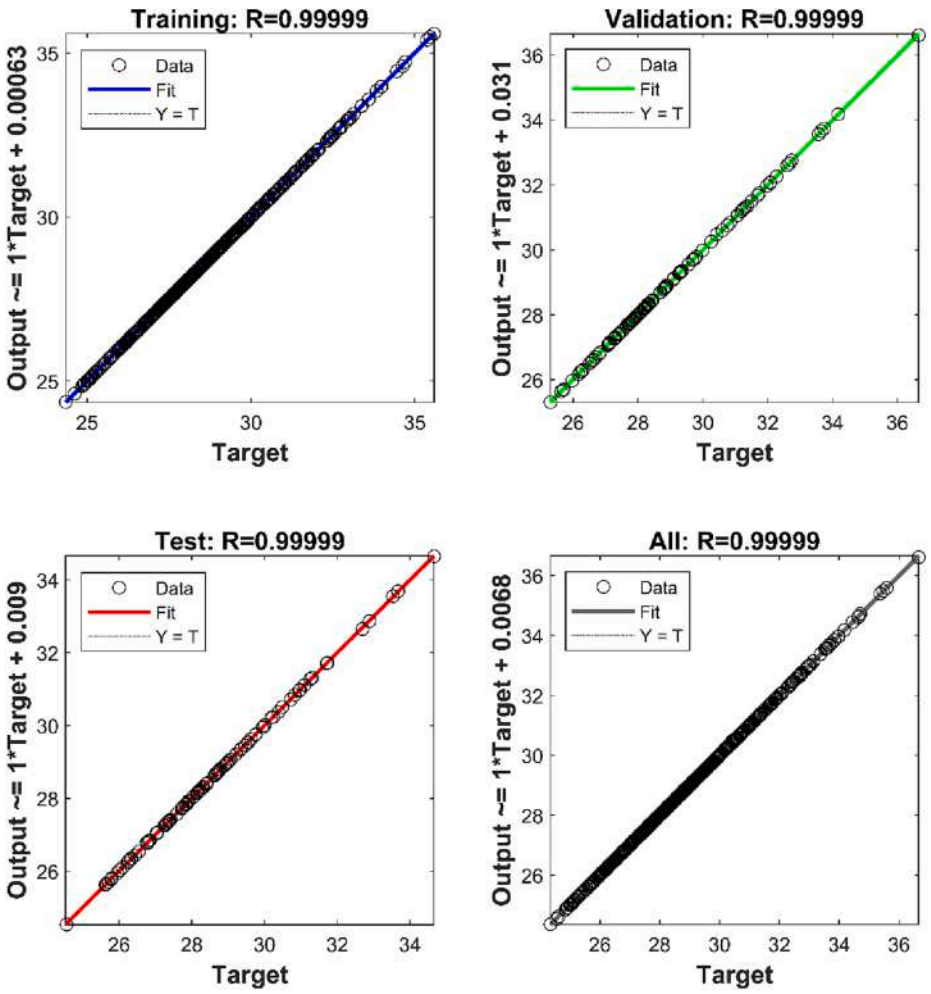

Fig. 17. Validation of the ANN algorithm for the objective function (Cost).

because larger equipment will be needed also, as well as their repair and maintenance. As displayed in Fig. 12, the highest net output work of the four heat transfer fluids used in the PTSC is related to May. Moreover, the results show that Therminol 59 exhibits the best performance for use in PTSCs, among these fluids.

As shown in Fig. 13, the maximum exergy efficiency rate of the system is related to December and January. Based on the results, Therminol 59 is the best heat transfer fluid applied in the PTSC among others.

As shown in Fig. 14, the maximum energy efficiency of the system belongs to May. Furthermore, the results revealed that Therminol VP1 had the best energy efficiency in the PTSC, among the four applied heat transfer fluids. This heat transfer fluid manifests a reverse behavior and yields the best results in the solar collector in December.

Table 11 presents the computations associated with the system's net output work, produced cooling, freshwater, and hydrogen, as well as the energy and exergy efficiency averages investigated about the solar radiation intensity variations in Bandar Abbas for over a year.

5.4.1. Number of households supported by the system

Concerning the present study's results, related to the output power generation of the solar collector about the solar radiation of Bandar Abbas during the year, the number of households in which the system could support the required electric energy should be investigated. The International Energy Agency's statistics (2010) show that every Iranian family has a per capita consumption of approximately 2431 kWh per month. That is, the sum of the electric energy used by every Iranian family is gauged at 29,172 kWh per year. Herein, the number of households the system could supply electric energy to during the year to the solar radiation of Bandar Abbas city is calculated, in addition to four heat transfer fluids applied in the PTSC. The results of these calculations are listed in Table 12.

Concerning the heat transfer fluids analysis in PTSCs, the present study shows that Therminol 59 performs better than other fluids. As shown in Table 8, this is due to the higher specific heat capacity of Therminol 59 compared to other heat transfer fluids concerning the present system, and its suitable thermal stability.

5.5. Optimization

In the proposed system, an optimization procedure is implemented, with the Therminol 59 heat transfer fluid in the PTSCs, selected as the most performant in the previous section. The optimization is delineated as follows:

5.5.1. ANNs

ANNs are computational models based on the biological theory that contain a large number of computing elements (linear or nonlinear) called neurons. An ANN is a programmable method for learning from data. An initial set of neurons is linked so that they can send data to each other. Subsequently, a problem is identified in which the network must be solved. The network repeatedly attempts this process, verifying successful links and eliminating those that fail. With sufficient training samples and computing power, ANN can answer any question. The ability of ANNs to simulate and model nonlinear processes makes them

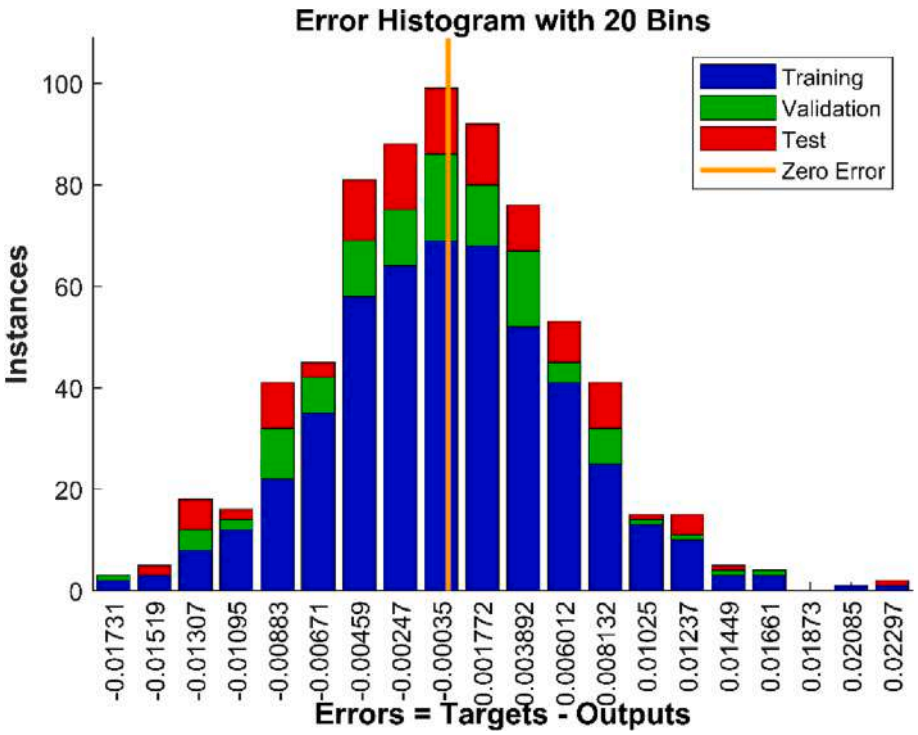

Fig. 18. ANN model error histogram.

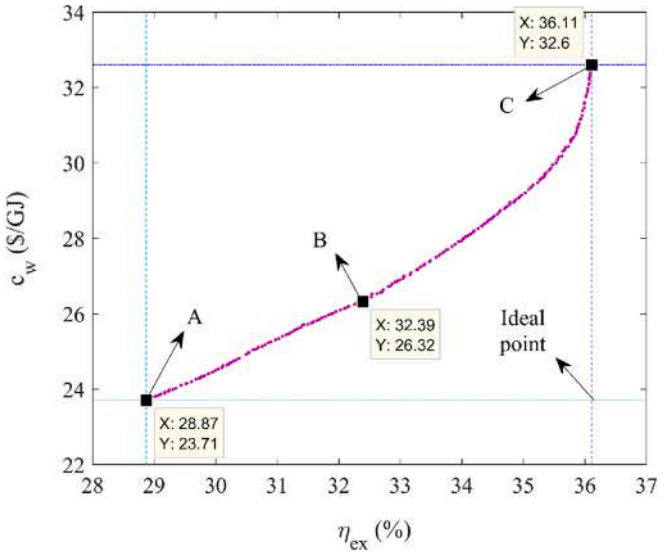

Fig. 19. Pareto front of the proposed system's optimal points.

useful in a variety of fields such as optimizing energy systems. A total of 700 samples from the input–output points were obtained from the results of the proposed thermodynamic analysis to train the network. Multiobjective optimization was performed on the trained network using the multiobjective non-dominated sorting genetic algorithm (NSGA-II). To determine the accuracy, the network determines the output results and the mean squared error (MSE). A significant advantage of the proposed method is the reduction in time because the thermodynamic calculations have to be performed only in the first step and not again during the optimization process. The optimization process is shown in Fig. 15**a**.

ANN architectures have various types. A multilayer neural network (MLP) was used in this study. Fig. 15**b** shows its general structure, indicating that an ANN has three layers: input, hidden, and output layers. Fig. 16 and Fig. 17 show the regression for the exergy efficiency and cost as objective functions.

Based on the simulated system shown in Fig. 16 and Fig. 17, the neural network has a high level of accuracy. Fig. 18 shows the ANN model error histogram of different data types. As shown in this figure, most of the data are near zero, indicating the high reliability of the network.

5.5.2. NSGA-II optimizer

The multi-objective optimization of NSGA_II was applied to the suggested combined energy system. All the solution points on the Pareto frontier (Fig. 19) are optimal. A decision-making process is required for the selection of the final optimal solution (providing the best tradeoff between objectives) among the optimal points; herein, a simple geometric method is employed.

As indicated in Fig. 19, a considerable decrease in costs can be achieved if the exergy efficiency is slightly compromised. The specifications for points 1, 2, and 3 are listed in Table 13**.** The population distribution is shown in Fig. 20 to illustrate the optimal point characteristics.

Table 13
Details related to points A, B, and C.

Point	T_1 (°C)	$\dot{m}_1$ ($\frac{kg}{s}$)	PP_{Eva} (°C)	P_7 (kPa)	T_{11} (°C)	η_{exergy} (%)	c_w ($/GJ)	W_{net} (kW)	$\dot{m}_{H2}$ ($\frac{kg}{h}$)
A	160.33	16.75	9.03	2002.8	90.22	28.87	23.71	991.4	2.62
B	160.57	15.43	3.44	2013.1	117.11	32.39	26.32	1140	3
C	179.98	19.97	3.03	2360.4	119.77	36.11	32.6	1407	3.67

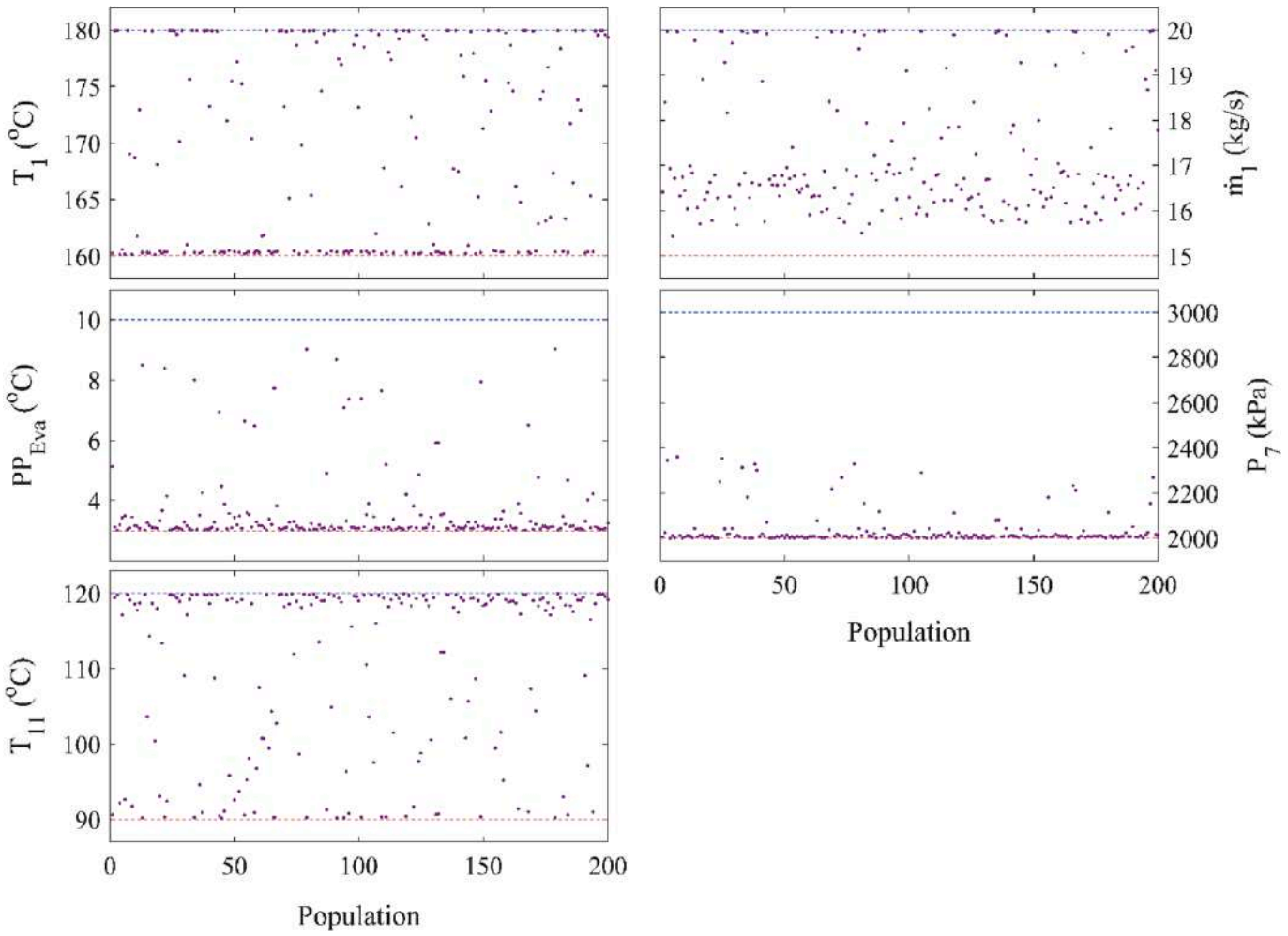

Fig. 20. Scatter distribution of the decision variables.

6. Conclusion

A polygene ration system was modeled and optimized in this study based on solar and geothermal renewable energies. This system produces electricity, cooling, freshwater, and hydrogen. The subsystems include parabolic trough solar collectors, steam Rankine cycle, organic Rankine cycle, PEM electrolyzer, and reverse osmosis desalination unit. Therminol 59, Marlotherm SH, Syltherm 800, and Therminol VP1 are different heat transfer fluids that were evaluated and assessed for selection in solar collectors. The thermodynamic EES software was used to solve the governing equations, model the system, and obtain the results derived from the parametric analysis of the system. By utilizing four types of heat transfer fluid in the parabolic trough solar collector, a parametric analysis was implemented for the solar radiation intensity, solar collector mass flow rate, turbine and pump efficiency, evaporator pinch-point temperature, and ORC turbine inlet temperature.

The summary of the results of this research can be stated as follows:

- Therminol 59 oil yielded the best result in terms of system outputs while ensuring the maximum cost.
- The results of examining the exergy destruction of the system revealed that the parabolic trough solar collector and pumps experienced the maximum and minimum exergy destruction in the system, respectively.
- The selected case study was Bandar Abbas owing to the city's suitable solar and geothermal energy potential.
- The effect of the temperature of the hottest and coldest days of the year on the system efficiency was explored.
- The results of the case study showed that the proposed system produces 5,741,637 kWh of electricity per year, supporting the energy needs of 196 households on average (for 1 year), with 1,935,794 kWh cooling; 169,803 m3 freshwater; and 15,371 kg of hydrogen.
- The system with the performant heat transfer fluid (i.e., Therminol 59) was optimized using the NSGA-II.
- The optimization results showed that the proposed system at the optimal point has an exergy efficiency of 32.39% and a cost rate of $36.32/GJ and produces 1140 kW of power.

Declaration of Competing Interest

The authors declare that they have no known competing financial interests or personal relationships that could have appeared to influence the work reported in this paper.

Data availability

Data will be made available on request.

Acknowledgement

This work was supported by the National Research Foundation of Korea (NRF) grant funded by the Korea government (MSIT) (2021R1A2C1092152).

References

[1] E.S. Sahin, I.S. Bayram, M. Koc, Demand side management opportunities, framework, and implications for sustainable development in resource-rich countries: Case study Qatar, J. Clean. Prod. 241 (2019), 118332, https://doi.org/10.1016/j.jclepro.2019.118332.

[2] I.B. Fridleifsson, Geothermal energy for the benefit of the people, Renew. Sustain. Energy Rev. 5 (3) (2001) 299–312, https://doi.org/10.1016/S1364-0321(01)00002-8.

[3] M.I. Alhamid, Y. Daud, A. Surachman, et al., Potential of geothermal energy for electricity generation in Indonesia: A review, Renew. Sustain. Energy Rev. 53 (2016) 733–740, https://doi.org/10.1016/j.rser.2015.09.032.

[4] J.W. Lund, T.L. Boyd, Direct utilization of geothermal energy 2015 worldwide review, Geothermics 60 (2016) 66–93, https://doi.org/10.1016/j.geothermics.2015.11.004.

[5] V. Stefansson, World geothermal assessment, Proceedings world geothermal congress. 2005, 2005, pp. 24-29.

[6] K.M. Powell, K. Rashid, K. Ellingwood, et al., Hybrid concentrated solar thermal power systems: A review, Renew. Sustain. Energy Rev. 80 (2017) 215–237.

[7] Q. Wang, H. Yang, S. Zhong, et al., Comprehensive experimental testing and analysis on parabolic trough solar receiver integrated with radiation shield, Appl. Energy 268 (2020), 115004, https://doi.org/10.1016/j.rser.2017.05.067.

[8] H. Naik, P. Baredar, A. Kumar, Medium temperature application of concentrated solar thermal technology: Indian perspective, Renew. Sustain. Energy Rev. 76 (2017) 369–378, https://doi.org/10.1016/j.rser.2017.03.014.

[9] Y. Qiu, Y. Xu, Q. Li, et al., Efficiency enhancement of a solar trough collector by combining solar and hot mirrors, Appl. Energy 299 (2021), 117290, https://doi.org/10.1016/j.apenergy.2021.117290.

[10] Q. Wang, B. Shen, J. Huang, et al., A spectral self-regulating parabolic trough solar receiver integrated with vanadium dioxide-based thermochromic coating, Appl. Energy 285 (2021), 116453, https://doi.org/10.1016/j.apenergy.2021.116453.

[11] A. Sharma, A.K. Shukla, O. Singh, et al., Recent advances in gas/steam power cycles for concentrating solar power, Int. J. Ambient Energy (2021) 1–12, https://doi.org/10.1080/01430750.2021.1919552.

[12] Q. Wang, G. Pei, H. Yang, Techno-economic assessment of performance-enhanced parabolic trough receiver in concentrated solar power plants, Renew. Energy 167 (2021) 629–643, https://doi.org/10.1016/j.renene.2020.11.132.

[13] P. Li, J. Li, G. Pei, et al., A cascade organic Rankine cycle power generation system using hybrid solar energy and liquefied natural gas, Sol. Energy 127 (2016) 136–146, https://doi.org/10.1016/j.solener.2016.01.029.

[14] J. Asadi, P. Amani, M. Amani, et al., Thermo-economic analysis and multi-objective optimization of absorption cooling system driven by various solar collectors, Energ. Conver. Manage. 173 (2018) 715–727, https://doi.org/10.1016/j.enconman.2018.08.013.

[15] P. Heidarnejad, H. Genceli, M. Asker, S. Khanmohammadi, A comprehensive approach for optimizing a biomass assisted geothermal power plant with freshwater production: Techno-economic and environmental evaluation, Energy Convers Manag 226 (2020), 113514, https://doi.org/10.1016/j.enconman.2020.113514.

[16] M. Kahraman, A.B. Olcay, E. Sorgüven, Thermodynamic and thermoeconomic analysis of a 21 MW binary type air-cooled geothermal power plant and determination of the effect of ambient temperature variation on the plant performance, Energy Convers Manag 192 (2019) 308–320, https://doi.org/10.1016/j.enconman.2019.04.036.

[17] H. Kianfard, S. Khalilarya, S. Jafarmadar, Exergy and exergoeconomic evaluation of hydrogen and distilled water production via combination of PEM electrolyzer, RO desalination unit and geothermal driven dual fluid ORC, Energy Convers Manag 177 (2018) 339–349, https://doi.org/10.1016/j.enconman.2018.09.057.

[18] S.M. Alirahmi, E. Assareh, A. Chitsaz, S.G. Holagh, S. Jalilinasrabady, Electrolyzer-fuel cell combination for grid peak load management in a geothermal power plant: Power to hydrogen and hydrogen to power conversion, Int J Hydrogen Energy 46 (2021) 25650–25665, https://doi.org/10.1016/j.ijhydene.2021.05.082.

[19] S. Hu, Z. Yang, J. Li, Y. Duan, Thermo-economic optimization of the hybrid geothermal-solar power system: A data-driven method based on lifetime off-design operation, Energy Convers Manag 229 (2021), 113738, https://doi.org/10.1016/j.enconman.2020.113738.

[20] E.D. Kerme, J. Orfi, A.S. Fung, E.M. Salilih, S.-U.-D. Khan, H. Alshehri, et al., Energetic and exergetic performance analysis of a solar driven power, desalination and cooling poly-generation system, Energy 196 (2020), 117150, https://doi.org/10.1016/j.energy.2020.117150.

[21] E. Assareh, S.M. Alirahmi, P. Ahmadi, A Sustainable model for the integration of solar and geothermal energy boosted with thermoelectric generators (TEGs) for electricity, cooling and desalination purpose, Geothermics 92 (2021), 102042, https://doi.org/10.1016/j.geothermics.2021.102042.

[22] D.K. Gupta, R. Kumar, N. Kumar, Performance analysis of PTC field based ejector organic Rankine cycle integrated with a triple pressure level vapor absorption system (EORTPAS), Eng Sci Technol an Int J 23 (2020) 82–91, https://doi.org/10.1016/j.jestch.2019.04.008.

[23] E. Assareh, S. Hoseinzadeh, D.E. Ghersi, et al., Energy, exergy, exergoeconomic, exergoenvironmental, and transient analysis of a gas-fired power plant-driven proposed system with combined Rankine cycle: thermoelectric for power production under different weather conditions, J Therm Anal Calorim (2022), https://doi.org/10.1007/s10973-022-11651-7.

[24] S.M. Alirahmi, E. Assareh, Energy, exergy, and exergoeconomics (3E) analysis and multi-objective optimization of a multi-generation energy system for day and night time power generation - Case study: Dezful city, Int J Hydrogen Energy 45 (2020) 31555–31573, https://doi.org/10.1016/j.ijhydene.2020.08.160.

[25] E. Bellos, C. Tzivanidis, K.A. Antonopoulos, A detailed working fluid investigation for solar parabolic trough collectors, Appl Therm Eng 114 (2017) 374–386, https://doi.org/10.1016/J.APPLTHERMALENG.2016.11.201.

[26] M. Shafiey Dehaj, M. Rezaeian, D. Mousavi, S. Shamsi, M. Salarmofrad, Efficiency of the parabolic through solar collector using $NiFe_2O_4$/Water nanofluid and U-tube, J Taiwan Inst Chem Eng 120 (2021) 136–149, https://doi.org/10.1016/J.JTICE.2021.02.029.

[27] M. Malekan, A. Khosravi, S. Syri, Heat transfer modeling of a parabolic trough solar collector with working fluid of Fe_3O_4 and CuO/Therminol 66 nanofluids under magnetic field, Appl Therm Eng 163 (2019), 114435, https://doi.org/10.1016/J.APPLTHERMALENG.2019.114435.

[28] R. Malviya, A. Agrawal, P.V. Baredar, A comprehensive review of different heat transfer working fluids for solar thermal parabolic trough concentrator, Mater Today Proc (2020), https://doi.org/10.1016/J.MATPR.2020.09.240.

[29] A. Naderipour, A. Abdullah, M.H. Marzbali, R. Ebrahimi, H. Kamyab, S. A. Nowdeh, J.J. Klemeš, S. Chelliapan, Optimal design of hybrid grid-connected photovoltaic/wind/battery sustainable energy system improving reliability, cost and emission, Energy (2022), https://doi.org/10.1016/j.energy.2022.124679.

[30] L. Gai, P.S. Varbanov, Y. Van Fan, J.J. Klemeš, S. Nižetić, Total Site Hydrogen Integration with fresh hydrogen of multiple quality and waste hydrogen recovery in refineries, Int. J. Hydrogen Energy 47 (24) (2022) 12159–12178, https://doi.org/10.1016/j.ijhydene.2021.06.154.

[31] M.I. Khan, M.H. Sutanto, K. Khan, M. Iqbal, M.B. Napiah, S.E. Zoorob, J. J. Klemeš, A. Bokhari, W. Rafiq, Effective use of recycled waste PET in cementitious grouts for developing sustainable semi-flexible pavement surfacing using artificial neural network (ANN), J. Clean. Prod. (2022), https://doi.org/10.1016/j.jclepro.2022.130840.

[32] H. Mikulčić, Z. Zhang, J. Baleta, J.J. Klemeš, Sustainable development in period of COVID-19 pandemic, J. Clean. Prod. (2021), https://doi.org/10.1016/j.jclepro.2021.129577.

[33] D. Fózer, A.J. Tóth, P.S. Varbanov, J.J. Klemeš, P. Mizsey, Sustainability assessment of biomethanol production via hydrothermal gasification supported by artificial neural network, J. Clean. Prod. (2021), https://doi.org/10.1016/j.jclepro.2021.128606.

[34] A.K. Tiwari, V. Kumar, Z. Said, H.K. Paliwal, A review on the application of hybrid nanofluids for parabolic trough collector: Recent progress and outlook, J. Clean. Prod. 292, 126031.

[35] Z. Said, M. H. Sajid, R. Saidur, G. A. Mahdiraji, N. A. Rahim, evaluating the optical properties of tio2 nanofluid for a direct absorption solar collector, Numerical Heat Transfer, Part A: Appl. 67 (9), 1010-1027.

[36] H. Li, Y. Zhang, C. Li, Z. Zhou, X. Nie, Y. Chen, H. Cao, B. Liu, N. Zhang, Z. Said, Extreme pressure and antiwear additives for lubricant: academic insights and perspectives, Int. J. Adv. Manufacturing Technol., 1-27.

[37] L.S. Sundar, Y.T. Sintie, Z. Said, M.K. Singh, V. Punnaiah, A.C.M. Sousa, Energy, efficiency, economic impact, and heat transfer aspects of solar flat plate collector with Al2O3 nanofluids and wire coil with core rod inserts, Sustainable Energy Technol. Assess. 40, 100772.

[38] E. Bellos, C. Tzivanidis, Z. Said, A systematic parametric thermal analysis of nanofluid-based parabolic trough solar collectors, Sustainable Energy Technol. Assess. 39, 100714.

[39] M.A. Abdelkareem, A. Allagui, E.T. Sayed, M.E.H. Assad, Z. Said, K. Elsaid, Comparative analysis of liquid versus vapor-feed passive direct methanol fuel cells, Renewable Energy 131, 563-584.

[40] A. Sohani, S. Naderi, F. Torabi, H. Sayyaadi, Y.G. Akhlaghi, X. Zhao, Application based multi-objective performance optimization of a proton exchange membrane fuel cell, J. Clean. Prod. 252, 119567.

[41] Z. Said, A.A. Alshehhi, A. Mehmood, Predictions of UAE's renewable energy mix in 2030, Renewable energy 118, 779-789.

[42] Z. Said, A. Kamyar, R. Saidur, Experimental investigation on the stability and density of TiO2, Al2O3, SiO2 and TiSiO4, IOP conference series: earth and environmental science 16 (1), 012002.

[43] X. Wang, C. Li, Y. Zhang, Z. Said, S. Debnath, S. Sharma, M. Yang, T. Gao, Influence of texture shape and arrangement on nanofluid minimum quantity lubrication turning, Int. J. Adv. Manufacturing Technol. 119 (1), 631-646.

[44] S. Rahman, S. Issa, Z. Said, M.E.H. Assad, R. Zadeh, Y. Barani, Performance enhancement of a solar powered air conditioning system using passive techniques and SWCNT/R-407c nano refrigerant, Case Stud. Therm. Eng. 16, 100565.

[45] L.S. Sundar, S. Mesfin, E.V. Ramana, Z. Said, A.C.M. Sousa, Experimental investigation of thermo-physical properties, heat transfer, pumping power, entropy generation, and exergy efficiency of nanodiamond+ Fe3O4/60: 40% water-ethylene, Therm. Sci. Eng. Prog. 21, 100799.

[46] A. Kumar, A.K. Tiwari, Z. Said, A comprehensive review analysis on advances of evacuated tube solar collector using nanofluids and PCM, Sustainable Energy Technol. Assess. 47, 101417.

[47] M. Ghodbane, E. Bellos, Z. Said, B. Boumeddane, A.K. Hussein, L. Kolsi, Evaluating energy efficiency and economic effect of heat transfer in copper tube for small solar linear Fresnel reflector, J. Therm. Analy. Calorimetry, 1-19.

[48] Z. Said, A. Mehmood, Standalone photovoltaic system assessment for major cities of United Arab Emirates based on simulated results, J. Clean. Prod. 142, 2722-2729.

[49] A.T. Hoang, Z.H. Huang, S. Nižetić, A. Pandey, X.P. Nguyen, R. Luque, Characteristics of hydrogen production from steam gasification of plant-

originated lignocellulosic biomass and its prospects in Vietnam, Int. J. Hydrogen Energy.
[50] F. Hassan, F. Jamil, A. Hussain, H.M. Ali, M.M. Janjua, S. Khushnood, Recent advancements in latent heat phase change materials and their applications for thermal energy storage and buildings: A state of the art review, Sustainable Energy Technol. Assess. 49, 101646.
[51] Z. Said, N.K. Cakmak, P. Sharma, L.S. Sundar, A. Inayat, O. Keklikcioglu, C. Li, Synthesis, stability, density, viscosity of ethylene glycol-based ternary hybrid nanofluids: Experimental investigations and model-prediction using modern machine learning, Powder Technol. 400, 117190.
[52] Z. Said, M. Ghodbane, B. Boumeddane, A.K. Tiwari, L.S. Sundar, C. Li, Energy, exergy, economic and environmental (4E) analysis of a parabolic trough solar collector using MXene based silicone oil nanofluids, Solar Energy Mater. Solar Cells 239, 111633.
[53] Z. Said, M. Ghodbane, A.A. Hachicha, B. Boumeddane, Optical performance assessment of a small experimental prototype of linear Fresnel reflector, Case Stud. Therm. Eng. 16, 100541.
[54] Y. Ahmadi, A.M. Asadi, M.J. Amani, X. Yu, Resilient Model Predictive Adaptive Control of Networked Z-Source Inverters Using GMDH, IEEE Trans. Smart Grid 13 (5) (Sept. 2022) 3723–3734, https://doi.org/10.1109/TSG.2022.3174250.
[55] M. Ahmadi, S. Nabipour, B.-I. Taheri, V. Vahidinasab, A New False Data Injection Attack Detection Model for Cyberattack Resilient Energy Forecasting, IEEE Trans. Ind. Inf. 19 (1) (Jan. 2023) 371–381, https://doi.org/10.1109/TII.2022.3151748.
[56] A. Arjomandi-Nezhad, S. Ahmadi, M. Taheri, M.-A. Fotuhi-Firuzabad, M. Lehtonen, Pandemic-Aware Day-Ahead Demand Forecasting Using Ensemble Learning, IEEE Access 10 (2022) 7098–7106, https://doi.org/10.1109/ACCESS.2022.3142351.
[57] R. Dhivagar, et al., A case study on thermal performance analysis of a solar still basin employing ceramic magnets, Case Stud. Therm. Eng. 39 (2022), 102402.
[58] A. Khademi, et al., A brief review on different hybrid methods of enhancement within latent heat storage systems, J. Storage Mater. 54 (2022), 105362.
[59] M.K. Sarangi, et al., Hydrothermal behavior and irreversibility analysis of Bödewadt flow of radiative and dissipative ternary composite nanomaterial due to a stretched rotating disk, Mater. Sci. Eng. B 287 (2023), 116124.
[60] M. Imran et al., Chapter 19 - Exergoeconomic optimization of a binary geothermal power plant. Thermodynamic Analysis and Optimization of Geothermal Power Plants. C. O. Colpan, M. A. Ezan and O. Kizilkan, Elsevier, 2021, pp. 315-326.
[61] H.A. Muhammad, et al., Numerical Modeling of Ejector and Development of Improved Methods for the Design of Ejector-Assisted Refrigeration System, Energies 13 (2020), https://doi.org/10.3390/en13215835.
[62] H. Sultan, et al., Advanced post combustion CO2 capture process – A systematic approach to minimize thermal energy requirement, Appl. Therm. Eng. 184 (2021), 116285.
[63] M.A. Alazwari, et al., Effects of various types of nanomaterials on PCM melting process in a thermal energy storage system for solar cooling application using CFD and MCMC methods, Int. J. Heat Mass Transf. 195 (2022), 123204.
[64] A. Karimi, et al., Investigating the mechanical properties and fusion zone microstructure of dissimilar laser weld joint of duplex 2205 stainless steel and A516 carbon steel, Opt. Laser Technol. 158 (2023), 108875.
[65] X. Liu, et al., Phase change process in a porous Carbon-Paraffin matrix with different volume fractions of copper oxide Nanoparticles: A molecular dynamics study, J. Mol. Liq. 366 (2022), 120296.
[66] H. Maleki, et al., Improving shipboard electronics cooling system by optimizing the heat sinks configuration, J. Ocean. Eng. Sci. 7 (5) (2022) 498–508.
[67] M. Shahgholi, et al., Fabrication and characterization of synthesized hydroxyapatite/ethanolamine for bone tissue engineering application, Colloids Surf A Physicochem Eng Asp 650 (2022), 129591.
[68] M.R. ul Haq et al., 2022. Energy transport analysis of the magnetized forced flow of power-law nanofluid over a horizontal wall. J. Magnet. Magnet. Mater. 560, 169681.
[69] M. Ghalambaz, et al., Mathematical modeling of heterogeneous metal foams for phase-change heat transfer enhancement of latent heat thermal energy storage units, App. Math. Model. 115 (2023) 398–413.
[70] A. Nee, et al., Three-dimensional simulation of full conduction-convection-radiation coupling with high Rayleigh numbers, Int. J. Therm. Sci. 184 (2023), 107958.
[71] S. Rajput, et al., Unsteady axisymmetric flow of nanofluid on nonlinearly expanding surface with variable fluid properties, JCIS Open 8 (2022), 100064.
[72] E. Cuce, et al., Improving thermal performance of thermoelectric coolers (TECs) through a nanofluid driven water to air heat exchanger design: An experimental research, Energ. Conver. Manage. 214 (2020), 112893.
[73] P. Mert Cuce, et al., Effect of using hybrid nanofluids as a coolant on the thermal performance of portable thermoelectric refrigerators, Sustainable Energy Technol. Assess. 53 (2022), 102685.
[74] H. Shakibi, et al., Using machine learning approaches to model and optimize a combined solar/natural gas-based power and freshwater cogeneration system, Appl. Energy 333 (2023), 120607.
[75] H. Shakibi, et al., Exergoeconomic and optimization study of a solar and wind-driven plant employing machine learning approaches; a case study of Las Vegas city, J. Clean. Prod. 385 (2023), 135529.
[76] E. Assareh, et al., An integrated system for producing electricity and fresh water from a new gas-fired power plant and a concentrated solar power plant – Case study – (Australia, Spain, South Korea, Iran), Renewable Energy Focus 44 (2023) 19–39.
[77] E. Assareh, et al., Transient thermodynamic modeling and economic assessment of cogeneration system based on compressed air energy storage and multi-effect desalination, J. Storage Mater. 55 (2022), 105683.
[78] A. Dezhdar, et al., A transient model for clean electricity generation using Solar energy and ocean thermal energy conversion (OTEC) - case study: Karkheh dam - southwest Iran, Energy Nexus 100176 (2023).
[79] P. Pourmoghadam, A. Kasaeian, Economic and energy evaluation of a solar multi-generation system powered by the parabolic trough collectors, Energy 262 (2023), 125362.
[80] A.E. Karaca, et al., Development of an integrated solar and wind driven energy system for desalination and power generation, Sustainable Energy Technol. Assess. 52 (2022), 102249.
[81] A.R. Razmi, et al., A green hydrogen energy storage concept based on parabolic trough collector and proton exchange membrane electrolyzer/fuel cell: Thermodynamic and exergoeconomic analyses with multi-objective optimization, Int. J. Hydrogen Energy 47 (62) (2022) 26468–26489.
[82] O. Rejeb, et al., Innovative integrated solar powered polygeneration system for green Hydrogen, Oxygen, electricity and heat production, Energ. Conver. Manage. 269 (2022), 116073.
[83] N. Nedaei, et al., Performance assessment and multi-objective optimization of a multi-generation system based on solar tower power: A case study in Dubai, UAE, Process Saf. Environ. Prot. 161 (2022) 295–315.
[84] Y.E. Yüksel, Thermodynamic assessment of modified Organic Rankine Cycle integrated with parabolic trough collector for hydrogen production, Int J Hydrogen Energy 43 (2018) 5832–5841, https://doi.org/10.1016/j.ijhydene.2017.09.164.
[85] S.A. Kalogirou, Solar Energy Engineering - Processes and Systems. 2nd Edition. Academic Press, 2013.
[86] F.A. Al-Sulaiman, Exergy analysis of parabolic trough solar collectors integrated with combined steam and organic Rankine cycles, Energy Convers Manag 77 (2014) 441–449, https://doi.org/10.1016/j.enconman.2013.10.013.
[87] S.A. Mousavi, M. Mehrpooya, M. Delpisheh, Development and life cycle assessment of a novel solar-based cogeneration configuration comprised of diffusion-absorption refrigeration and organic Rankine cycle in remote areas, Process Saf Environ Prot 159 (2022) 1019–1038, https://doi.org/10.1016/J.PSEP.2022.01.067.
[88] F.A. Boyaghchi, M. Chavoshi, V. Sabeti, Multi-generation system incorporated with PEM electrolyzer and dual ORC based on biomass gasification waste heat recovery: Exergetic, economic and environmental impact optimizations, Energy 145 (2018) 38–51, https://doi.org/10.1016/j.energy.2017.12.118.
[89] S.M. Alirahmi, S. Rahmani Dabbagh, P. Ahmadi, S. Wongwises, Multi-objective design optimization of a multi-generation energy system based on geothermal and solar energy, Energy Convers Manag 205 (2020), 112426, https://doi.org/10.1016/j.enconman.2019.112426.
[90] B. Zhang, Y. Chen, Z. Wang, H. Shakibi, Thermodynamic, environmental, and optimization of a new power generation system driven by a gas turbine cycle, Energy Rep. 6 (2020) 2531–2548, https://doi.org/10.1016/j.egyr.2020.09.003.
[91] M. Delpisheh, M.A. Haghghi, H. Athari, M. Mehrpooya, Desalinated water and hydrogen generation from seawater via a desalination unit and a low temperature electrolysis using a novel solar-based setup, Int J Hydrogen Energy 46 (2021) 7211–7229, https://doi.org/10.1016/j.ijhydene.2020.11.215.
[92] M. Delpisheh, M. Abdollahi Haghghi, M. Mehrpooya, A. Chitsaz, H. Athari, Design and financial parametric assessment and optimization of a novel solar-driven freshwater and hydrogen cogeneration system with thermal energy storage, Sustain Energy Technol Assessments 45 (2021), 101096, https://doi.org/10.1016/j.seta.2021.101096.
[93] M. Mehrpooya, M. Raeesi, F. Pourfayaz, M. Delpisheh, Investigation of a hybrid solar thermochemical water-splitting hydrogen production cycle and coal-fueled molten carbonate fuel cell power plant, Sustain Energy Technol Assessments 47 (2021), 101458, https://doi.org/10.1016/J.SETA.2021.101458.
[94] H. Rashidi, J. Khorshidi, Exergoeconomic analysis and optimization of a solar based multigeneration system using multiobjective differential evolution algorithm, J Clean Prod 170 (2018) 978–990, https://doi.org/10.1016/j.jclepro.2017.09.201.
[95] A. Nemati, M. Sadeghi, M. Yari, Exergoeconomic analysis and multi-objective optimization of a marine engine waste heat driven RO desalination system integrated with an organic Rankine cycle using zeotropic working fluid, Desalination 422 (2017) 113–123, https://doi.org/10.1016/j.desal.2017.08.012.
[96] A. Naseri, M. Bidi, M.H. Ahmadi, R. Saidur, Exergy analysis of a hydrogen and water production process by a solar-driven transcritical CO2 power cycle with Stirling engine, J Clean Prod 158 (2017) 165–181, https://doi.org/10.1016/j.jclepro.2017.05.005.
[97] A.R. Razmi, M. Janbaz, Exergoeconomic assessment with reliability consideration of a green cogeneration system based on compressed air energy storage (CAES), Energy Convers Manag 204 (2020), 112320, https://doi.org/10.1016/j.enconman.2019.112320.
[98] I. Dincer, M.A. Rosen, P. Ahmadi, Optimization of energy systems, Optim Energy Syst (2017) 1–453, https://doi.org/10.1002/9781118894484.
[99] M. Mehrpooya, P. Bahramian, F. Pourfayaz, H. Katooli, M. Delpisheh, A novel hybrid liquefied natural gas process with absorption refrigeration integrated with molten carbonate fuel cell, Int J Low-Carbon Technol (2021), https://doi.org/10.1093/ijlct/ctab021.
[100] E. Assareh, M. Delpisheh, E. Farhadi, W. Peng, H. Moghadasi, Optimization of geothermal- and solar-driven clean electricity and hydrogen production multi-generation systems to address the energy nexus, Energy Nexus 5 (2022), 100043, https://doi.org/10.1016/J.NEXUS.2022.100043.

[101] T. Parikhani, M. Delpisheh, M.A. Haghghi, S.G. Holagh, H. Athari, Performance enhancement and multi-objective optimization of a double-flash binary geothermal power plant, Energy Nexus 100012 (2021), https://doi.org/10.1016/J.NEXUS.2021.100012.
[102] H. Montazerinejad, P. Ahmadi, Z. Montazerinejad, Advanced exergy, exergo-economic and exrgo-environmental analyses of a solar based trigeneration energy system, Appl Therm Eng 152 (2019) 666–685, https://doi.org/10.1016/j.applthermaleng.2019.01.040.
[103] S.M. Alirahmi, S. Rahmani Dabbagh, P. Ahmadi, S. Wongwises, H. Kianfard, S. Khalilarya, et al., Multi-criteria design optimization and thermodynamic analysis of a novel multi-generation energy system for hydrogen, cooling, heating, power, and freshwater, Energy Convers Manag 45 (2020) 5832–5841, https://doi.org/10.1016/j.enconman.2020.113514.
[104] E. Assareh, M. Delpisheh, S.M. Alirahmi, S. Tafi, M. Carvalho, Thermodynamic-economic optimization of a solar-powered combined energy system with desalination for electricity and freshwater production, Smart Energy 5 (2022), 100062, https://doi.org/10.1016/J.SEGY.2021.100062.
[105] A.S. Nafey, M.A. Sharaf, Combined solar organic Rankine cycle with reverse osmosis desalination process: Energy, exergy, and cost evaluations, Renew Energy 35 (2010) 2571–2580, https://doi.org/10.1016/j.renene.2010.03.034.
[106] T. Ioroi, K. Yasuda, Z. Siroma, N. Fujiwara, Y. Miyazaki, Thin film electrocatalyst layer for unitized regenerative polymer electrolyte fuel cells, J Power Sources 112 (2002) 583–587, https://doi.org/10.1016/S0378-7753(02)00466-4.
[107] Y. Noorollahi, A. Golshanfard, S. Ansaripour, A. Khaledi, M. Shadi, Solar energy for sustainable heating and cooling energy system planning in arid climates, Energy 218 (2021), 119421, https://doi.org/10.1016/j.energy.2020.119421.
[108] H. Yousefi, Y. Noorollahi, S. Ehara, R. Itoi, A. Yousefi, Y. Fujimitsu, et al., Developing the geothermal resources map of Iran, Geothermics 39 (2010) 140–151, https://doi.org/10.1016/J.GEOTHERMICS.2009.11.001.
[109] Meteonorm Software Worldwide irradiation data, Global Meteorological Database for Engineers, Planners and Education. Meteotest AG, Fabrikstrasse 14 3012 Bern, Switz 2021. https://meteonorm.com/en/ (accessed May 13, 2021).